Journal of Turbulence

ISSN: (Print) (Online) Journal homepage: www.tandfonline.com/journals/tjot20

Challenges and perspective on the modelling of high-Re, incompressible, non-equilibrium, rough-wall boundary layers

Ricardo García-Mayoral, Daniel Chung, Paul Durbin, Nicholas Hutchins, Tobias Knopp, Beverley J. McKeon, Ugo Piomelli & Richard D. Sandberg

To cite this article: Ricardo García-Mayoral, Daniel Chung, Paul Durbin, Nicholas Hutchins, Tobias Knopp, Beverley J. McKeon, Ugo Piomelli & Richard D. Sandberg (04 Jun 2024): Challenges and perspective on the modelling of high-Re, incompressible, non-equilibrium, rough-wall boundary layers, Journal of Turbulence, DOI: 10.1080/14685248.2024.2361738

To link to this article: https://doi.org/10.1080/14685248.2024.2361738

Published online: 04 Jun 2024.

JOURNAL OF TURBULENCE
https://doi.org/10.1080/14685248.2024.2361738

Challenges and perspective on the modelling of high-Re, incompressible, non-equilibrium, rough-wall boundary layers

Ricardo García-Mayoral[a], Daniel Chung[b], Paul Durbin[c], Nicholas Hutchins[b], Tobias Knopp[d], Beverley J. McKeon[e], Ugo Piomelli[f] and Richard D. Sandberg[b]

[a]Dept. of Engineering, University of Cambridge, Cambridge, UK; [b]Dept. of Mechanical Engineering, University of Melbourne, Victoria, Australia; [c]Aerospace Engineering, Iowa State University, Ames, IA, USA; [d]Institut für Aerodynamik und Strömungstechnik, Deutsches Zentrum für Luft- und Raumfahrt (DLR), Göttingen, Germany; [e]Mechanical Engineering, Stanford University, Stanford, CA, USA; [f]Dept. of Mechanical and Materials Engineering, Queen's University, Kingston, ON, Canada

ABSTRACT

The present paper gives an overview of the recent modelling activities under NATO-STO AVT-349, focussed on the understanding and modelling of boundary layers for incompressible, high-Reynolds-number flows subject to non-equilibrium conditions such as strong pressure gradients, three-dimensionality, and surface roughness and heterogeneity. For this, we consider simpler cases where the above flow conditions are present separately or in a reduced number of combinations. First, we focus on the effect of roughness on the outer flow and the problems associated to its characterisation and prediction, with a particular emphasis on the conditions necessary for outer-layer similarity to hold. We then focus on how the presence of adverse and favourable pressure gradients affects the effect of roughness, and to what extent the figures used to quantify it are still useful under such conditions. We also consider the effect of surface heterogeneity, the shortcomings when modelling it and how these can be addressed. We then focus on the effect on the outer layer of pressure gradients and non-equilibrium conditions, to what extent similarity holds in those conditions, and how RANS models perform for such flows, identifying routes for their improvement to handle pressure gradients and non-equilibrium. We also discuss the use of data-driven and machine-aided methods in closure models.

ARTICLE HISTORY
Received 18 January 2024
Accepted 27 May 2024

KEYWORDS
Turbulence; boundary layer; roughness; non-equilibrium

1. Introduction

The accurate prediction of boundary layers is fundamental for successful vehicle design and operation in terms of drag, propulsion, manoeuvring and acoustics. Ever improving fluid-dynamics modelling and simulation tools are in constant demand in the naval and aviation sectors, as well as in the natural sciences, driven both by need and by the advance of computer technology. Over the years, the focus of incompressible boundary layer research has been, perhaps disproportionately, on low Reynolds numbers and idealised conditions. In the NATO-STO community, high-speed flows have seen a heavy emphasis on non-equilibrium problems in compressible boundary layers, generally aimed at aerodynamic applications. Comparatively, little attention has been paid to non-equilibrium boundary layers at conditions relevant to naval vehicles and low-speed manoeuvring air vehicles. To address this gap, NATO-STO Research Task Group AVT-349 was established to focus on boundary layers in realistic conditions, where both the Reynolds number is large and the surface has roughness, curvature and three-dimensionality, with regions of increasing and/or decreasing pressure, yet the flow is incompressible.

The objective of AVT-349 was to advance the accuracy and range of prediction models for such flows. This included establishing a database of coordinated experimental data-sets, with well-defined uncertainties and boundary conditions, that systematically address the non-equilibrium conditions found in practical applications; quantifying the limitations of current large-eddy simulation (LES) and Reynolds-Averaged Navier-Stokes (RANS) models; identifying the cases in which models based on new paradigms or with higher

CONTACT Ricardo García-Mayoral r.gmayoral@eng.cam.ac.uk

fidelity were required, and where they were not; and providing data, understanding and collaborations that would lead to the development of improved and/or new models.

Numerical simulations of full configurations of naval vehicles are a key element for design and performance assessment. Given the scale of the problem, a significant degree of modelling is always required; since the flow physics involved are rich and in some instances not fully understood, such simulations are challenging. The problem is compounded with the extremely large Reynolds number of applications, often 2–3 orders of magnitude larger than laboratory values. An example of a study of the full configuration, albeit at model Reynolds numbers, is given in a recent NATO-STO activity that has examined this problem [1]. For typical vehicle shapes, the complexity of the flow is exacerbated in manoeuvre and drift conditions. The development of unsteady vortices, their location and strength, for instance, influence the forces and moments acting on the hull, and thus its manoeuvring performance. In large ships such as tankers, the propeller operates in the wake flow building up over the stern, if not the full hull, of the ship. In these conditions it is of high importance for the propulsive efficiency of the vessel to be able to correctly predict this evolving boundary layer. The vortex development over the aft ship is deliberately controlled to direct as much of the velocity deficit created in the boundary layer into the propeller, again highlighting the practical importance of accurate predictions of this non-equilibrium boundary layer.

Present-day CFD solvers have difficulty capturing the essential features of such flows, not only quantitatively, but sometimes qualitatively too. An essential part of the problem is that the boundary layer around the vehicle is frequently far from the canonical conditions in which turbulence models are calibrated. The flow is subject to strong three-dimensionality, unsteadiness, tip and corner effects, pressure gradients, flow separation and sometimes transition, and the hull surface is hydraulically rough, often in an heterogeneous fashion, exhibiting large local friction coefficients. Conventional closures can struggle under such conditions. The development of new or improved models requires an in-depth understanding of the flow physics, but this first requires their breakdown into separate contributions, e.g. roughness, two-dimensional pressure-gradient effects, three-dimensionality effects, etc. The above discussion highlights the need to address a variety of flow features and mechanisms for the successful simulation of the flow around naval vehicles, starting with an understanding of the flow physics, which is the aim of this work.

The paper is organised as follows. Section 2 discusses roughness in the baseline case of equilibrium flows, the characterisation of its effect on skin-friction drag and some key aspects of the flow physics and how to model them. Section 3 then extends the discussion to the case of roughness under non-equilibrium conditions, caused either by the overlying flow being subject to pressure gradients or by surface heterogeneity. Section 4 discusses the non-equilibrium effects caused by flow three-dimensionality, essentially involving the effect of pressure gradients on the boundary layer. Finally, Section 5 summarises and concludes the paper.

2. Surface roughness in canonical flows

The effect of roughness on near-wall turbulence, and in particular its effect on skin friction and boundary layer thickness, is still not fully understood even for canonical flows with mild or zero pressure gradient and equilibrium conditions, i.e. channels, pipes and zero-pressure-gradient boundary layers. In theses cases, it is commonly accepted that, sufficiently far above the surface, the only effect of roughness on the overlying flow is a shift in the mean velocity profile, but that turbulence remains otherwise unaltered [2]. The mean velocity profile is then

$$U^+ = \frac{1}{\kappa}\log(y^+) + A - \Delta U^+, \tag{1}$$

where the $+$ superscript indicates viscous scaling, y^+ is the wall-normal distance, $\kappa \approx 0.39$ is the Kármán constant, $A \approx 5.1$ is the log-law intercept for a smooth-wall flow, and the roughness function, ΔU^+, is the velocity deficit caused by the roughness [3]. The latter propagates into the friction coefficient, $c_f = 2\tau_w/(\rho U_\delta^2) = 2/U_\delta^{+2}$, where U_δ is the velocity at the edge of the boundary layer, as it gives directly the decrease in U_δ^+. For a fixed surface geometry in viscous units, ΔU^+ would be given, and the change in drag would be straightforward to determine. The problem of roughness reduces then to the problem of determining ΔU^+.

The roughness function, however, can be difficult to predict *a priori* [4,5]. As illustrated in Figure 1(a), the roughness function for a given mean roughness height can vary greatly across roughness topologies, which

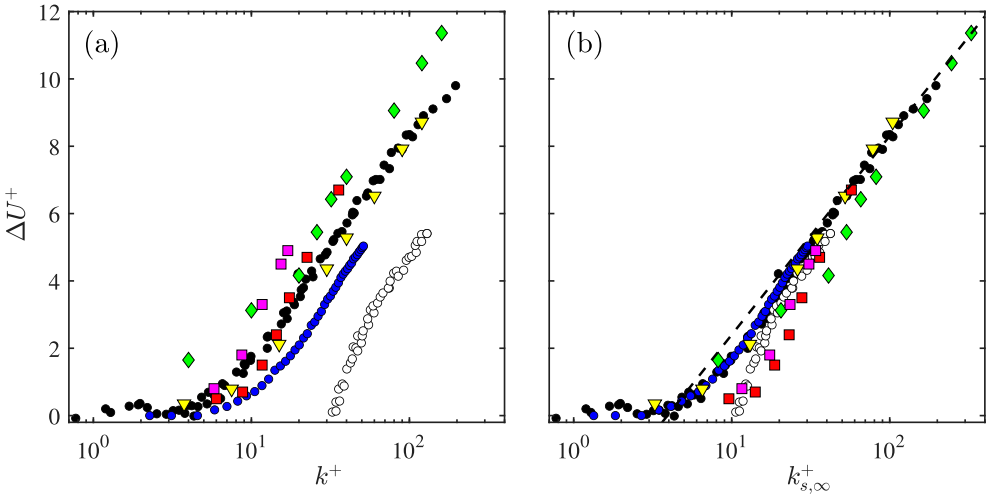

Figure 1. Offset of the mean velocity profile in viscous units, ΔU^+, for different roughness topologies, as a function of (a) the mean roughness height and (b) the equivalent sand-grain roughness, both also in viscous units, adapted from [5]. ● sand grains [8]; ○ tubeworms [9]; ● grit-blasted [10]; ▽ grit-blasted [11]; ◆ 3D sinusoids [12]; ■ square blocks [13]; ■ square blocks with staggered heights [13]. The dashed line is Equation (2).

do not exhibit a common behaviour. Most do, however, exhibit a common asymptotic trend for large roughness size, k^+, in what is known as the fully rough regime. In terms of friction coefficient, this is the regime where it becomes constant and independent of the Reynolds number in classical Moody charts [6]. The common asymptotic trend can be used to define an equivalent sand-grain roughness, such that a collapse of the roughness function can be observed in the latter regime for different topologies, as shown in Figure 1(b). The equivalent sand-grain roughness can be regarded in two ways. In one, its value in viscous units has a one-to-one correspondence to ΔU^+. When thus interpreted, we will denote it as k_s^+. In essence, k_s^+ is nothing but a different 'currency' that contains the same information as ΔU^+ [7], as given by

$$\Delta U^+ \approx \frac{1}{\kappa} \log(0.255 k_s^+), \tag{2}$$

and is therefore a hydrodynamic property that requires knowledge of the flow.

In the fully rough regime, the ratio k_s/k becomes constant. When we refer to sand-grain roughness in this regard, we will use the symbol $k_{s,\infty}^+$, to highlight that it is the value that k_s^+ tends to for large roughness. The lengthscale $k_{s,\infty}$ is then effectively a property of the surface geometry alone, but because it is still the asymptotic value of k_s for large k^+, it is still a hydrodynamic property. This becomes apparent in the difficulty to establish its dependence on the geometric properties of the roughness, but also in that the collapse observed in the fully rough regime does not extend to the transitionally rough regime of smaller roughness size [13], as shown in Figure 1(b) – or, alternatively, in k_s/k not being constant and varying across roughness topologies in the latter regime. Although it is common to use k_s^+ to characterise skin friction instead of ΔU^+ we note that small errors in the measurement of the mean velocity profile, and thus in ΔU^+, can lead to large deviations in k_s, so that k_s is a measure much more sensitive to variations than the actual figure of merit, ΔU^+. This is so because of the logarithmic character of their relation in Equation (2), such that, for instance, a 10% error in ΔU^+ can lead to a 25% deviation in the estimate of k_s at $\Delta U^+ \approx 6$, and to a 50% deviation at $\Delta U^+ \approx 10$. This augmentation in uncertainty from ΔU^+ to k_s^+ can be particularly severe when determining the equivalent sand-grain roughness from experimental measurements of the velocity profile. The uncertainty in the determination of the friction velocity can have a compound effect on this.

The typical existing methods to estimate k_s, ΔU^+ and skin friction for any given roughness geometry are discussed in this volume in [14]. Because these methods are generally of an *a posteriori* nature, that is, they rely on a database of measurements for a large but finite number of roughness configurations, they work relatively well when the roughness of interest is not too far off from those for which data exist. However, caution is needed when extrapolating to topologies that are significantly different.

Instead, the modelling tasks under AVT-349 have taken a different approach, aiming to develop *a priori* models, that is, not based on extrapolation of data for similar topologies, but from insight on the mechanisms through which that roughness alters the flow. The direct numerical simulations (DNSs) referenced in [14] were conducted to provide such insight. DNS is particularly well suited to study how near-wall turbulence is modified by small-scale roughness, as the simulation domains required to capture the physics correctly need not be particularly large, as discussed in Section 2.1, and the effect scales out to larger Reynolds numbers in viscous units. In particular, we have explored the possibility of *a priori* models for the roughness function based on the mechanisms identified in [13,15]. This work showed that the flow over textures can be decomposed into a texture-induced flow, coherent with the surface geometry, and a background turbulence which is essentially free of any footprint of texture, and therefore truly texture-incoherent. The first component is akin to the dispersive flow, although it is modulated in amplitude by the second, and vanishes quickly away from the wall. In turn, it modifies the background turbulence, which otherwise perceives the effect of surface texture through homogeneous, slip-like boundary conditions. Such conditions are typically derived using homogenisation techniques [16], taking the form of a linear, admittance relationship between the three velocity components and the shear and pressure stresses at a notional 'interface' plane, typically the roughness-crest plane. However, the application of these techniques to turbulent flows is significantly limited as soon as the roughness size is comparable to the overlying eddies, typically $k^+ \approx 15$. Beyond this size, the underlying assumption of separation of scales breaks down. Instead, [17] have analysed for the rough and porous surfaces of [18] the correlation between velocities and stresses at a notional interface plane for a broad range of lengthscales, without assuming scale separation. Hao and García-Mayoral [17] have found that those correlations agree well with the admittances obtained from simple, laminar-flow models for the flow below the interface in response to finite-scale interfacial stresses, as illustrated in Figure 2. The figure shows that the limit for separation of scales, $\lambda/L \to \infty$, can yield admittances of value significantly different to those effectively experienced by flow lengthscales 1–100 times larger than the texture spacing L, a range that typically covers all the active scales of turbulence near the wall. The figure also shows that assuming that the flow below the interface, in between the texture elements, is purely viscous, as is done in homogenisation, may be insufficient, and inertial terms should be retained, at a minimum in the form of temporal terms. This suggests a new, multi-scale framework to produce equivalent boundary conditions in the spirit of homogenisation, but addressing its limitations for turbulent flows.

Nevertheless, equivalent boundary conditions alone are sufficient to capture the effect of surface texture only up to sizes $k^+ \approx 15$, in the transitionally rough regime. Beyond this, the texture does not merely impose a boundary condition, but also induces additional stresses on the overlying flow, which result in a larger ΔU^+. Fairhall et al. [15] argued that these additional stresses are not merely the dispersive stress acting on the mean flow, but additional stresses acting on the fluctuations of the background turbulence, which arise from the non-linear interaction of the texture-coherent flow with the background turbulence through the advective terms in the momentum equations. This additional ΔU^+ is shown for idealised superhydrophobic textures in Figure 3. The surface topology consists of alternating regions of no slip, the solid posts, and free slip, the plastrons. This makes a particularly simple texture in terms of the corresponding effective boundary conditions and the dominant terms in the additional stresses [19], and thus a convenient benchmark to study the mechanisms at play. For the topology considered, results are shown for increasing texture spacing L^+, which is equivalent to varying the Reynolds number, and thus u_τ, in an experimental setup, and is a measure of texture size in the absence of a roughness height k_g^+. To investigate the additional-stresses mechanism, [19] have conducted texture-less simulations where the texture is replaced by the corresponding equivalent boundary conditions plus the cross-advective terms that result from the flow decomposition. Results for this model, compared with ΔU^+ from fully resolved, texture simulations, are also portrayed in Figure 3, exhibiting excellent agreement at least up to $L^+ \approx 50$. While these results have been obtained for a texture for which the model is particularly simple, mainly because a flat interface can be defined where the wall-normal velocity is identically zero, they show promise for the modelling of textures of sizes up to $L^+ \approx 50$, which would potentially cover the full transitionally rough regime and the onset of the fully rough regime for conventional roughness textures. Beyond that, the behaviour of ΔU^+ becomes common across topologies, as shown in Figure 1(b), so no further prediction for specific topologies would be needed.

Given a prescribed value of k_s^+ or ΔU^+, there are a number of techniques to model the effect of the assigned quantity at a macroscale level in RANS and LES simulations. Either of those quantities can, for

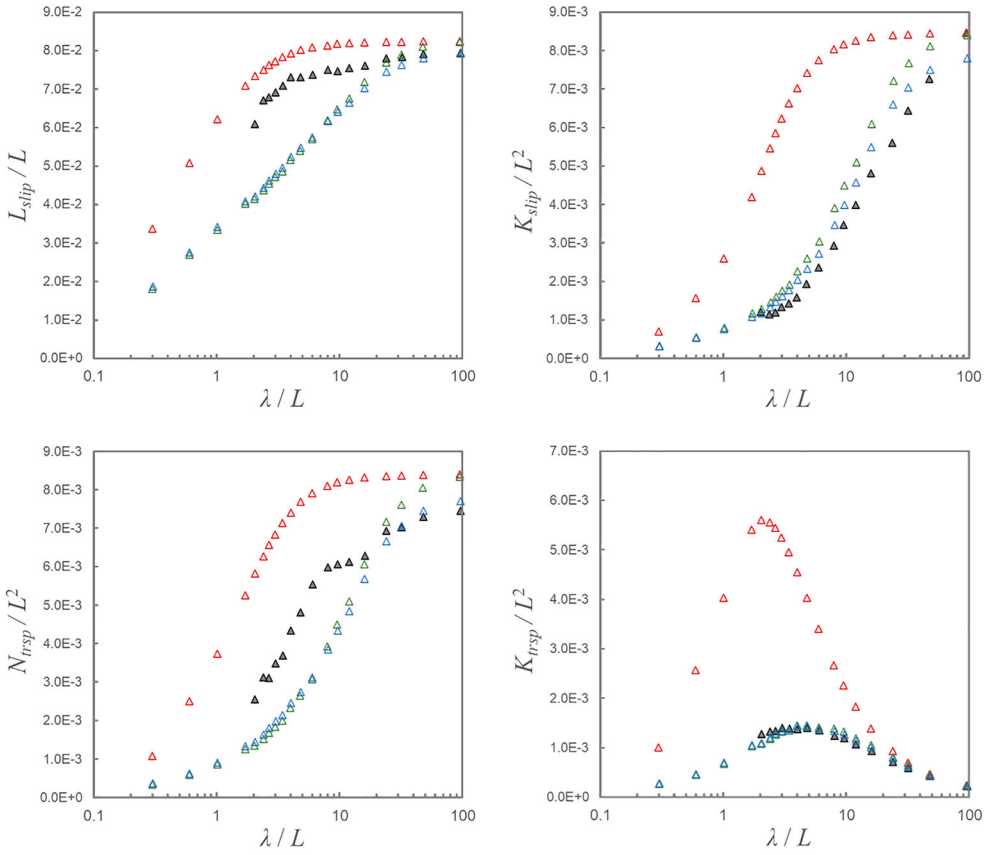

Figure 2. Observed and modelled shear-velocity magnitude correlations at the tip plane of a textured surface of element spacing L, for different wavelengths λ, from [17]. The assumed relationship is $u = L_{slip}\partial u/\partial y + K_{slip}p$ and $v = N_{trsp}\partial u/\partial y + K_{trsp}p$, so the coefficients L_{slip}, K_{slip}, N_{trsp} and K_{trsp} are the admittances relating velocities to stresses at a notional substrate/free-flow interface. Full symbols, results from DNS; red symbols, steady-Stokes model; green symbols, unsteady-Stokes model; blue symbols, linearised-Navier-Stokes model.

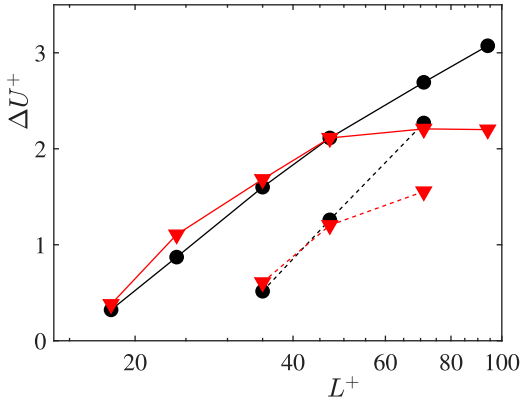

Figure 3. Roughness function caused by texture in superhydrophobic surfaces modelled as slip/no-slip patterns as a function of the texture spacing L^+, from [19]. Solid lines are for a collocated array of elements, and dashed lines for a staggered one. In black, results from fully resolved simulations. In red, results from texture-less simulations, where the effect of the texture has been modelled through texture-induced/background-turbulence cross advective terms.

instance be implemented into a wall model using distributed penalty forces [20], or through modifications of the Equilibrium-Stress-Layer (ESL) formulation, typically by changing the form of the log-law. Several ways of including this information for methods that solve the RANS equations have also been proposed [21–24]. These can then be used for simulations of full-scale vehicles [4,25], and it is even possible to use them in quick engineering calculations of the drag that use k_s as input and track the evolution of inner scaling along

the vehicle surface [26–28]. However, to use such models with confidence it is important to assess their validity when outer-layer similarity breaks down, in non equilibrium conditions, and when the surface roughness is heterogeneous.

2.1. Outer-layer similarity

In the classical description of wall turbulence, flows sufficiently far above rough and complex surfaces are generally believed to be essentially unaltered by the non-smooth wall, exhibiting outer-layer similarity with smooth-wall flows [2]. This picture has however been challenged by measurements of Kármán constants different from its nominal, smooth-wall value over different surfaces [29–39]. In principle, the Kármán constant arises from the matching of the outer solution, valid for $y^+ \gg 1$ and scaling with the free-stream velocity and the boundary layer thickness δ, and the inner solution, valid for $y \ll \delta$ and scaling with the friction velocity and the viscosity. The outer solution is typically observed to hold for $y^+ > 60$–100, and the inner one for $y < 0.2$–0.3δ. Provided there is enough scale separation between these two limits, the intermediate, overlapping region, the log layer, scales with u_τ and y, such that $\partial U/\partial y \propto 1/y$. The Kármán constant is then simply the constant of the proportionality in this relationship. There is no apparent reason why it should necessarily be the same for flows over different surfaces, given that it arises from the matching of different inner layers. However, there is some evidence that the log layer is self-sustaining and its core dynamics are independent of the underlying flow [40,41]. We would expect that, sufficiently far from the surface, information on the detail of the surface was lost and flow dynamics were independent of it.

That 'sufficiently far' height was proposed in [42] to be $\delta \gtrsim 40k$, based on the notion that the roughness layer, the region where the signature of individual roughness elements is noticeable in the flow, typically extends up to 2–3k, and that should be less than half of the thickness of the logarithmic layer. We would argue that, in order for a smooth-wall-like κ to manifest, a sufficient range of the log layer should be unaltered by the detail of the surface, and because of its logarithmic nature that should be at least half a decade, i.e. from 0.1δ to 0.3δ. This would imply $\delta \gtrsim 30k$, which is essentially the same figure of [42]. The above thresholds are consistent with the recent observation in experiments in [43] that, below $\delta \approx 40k$, the values of k_s/k obtained assuming outer layer similarity depart from its constant value at larger δ/k, suggesting a more in-depth alteration of the flow by the roughness. However, [44] notes that experiments and DNS show this to be overly conservative. An estimate of $\delta \gtrsim 15k$ has been found in experiments [45]. It was suggested that the reason this less stringent criterion is evident, is because roughness should be characterised by drag rather than geometrical height. The discrepancy in the limits above may however simply be due to what is sought in each case, whether it is the existence of a sufficiently deep log layer, on which a value for κ can be estimated with some confidence, or merely that the flow above the roughness layer exhibit outer layer similarity, regardless of the existence or not of a log layer. The variables and accuracy with which outer-layer-similarity is required will also affect the stringency of the criterion.

In any event, most naval applications satisfy these constraints, although care is needed when considering the early stages of the boundary layer, where this may not be the case. We note that there are other applications where this may also not be the case, e.g. atmospheric flows, where often $\delta \sim 10k$ [46,47]. In addition, there are surface topologies, typically with densely packed elements, where the roughness layer scales with the spacing rather than the height of the roughness [48,49]. For these topologies the relevant ratio would be between roughness spacing and δ, aiming in any event for the general criterion that the roughness layer be confined below 0.1δ.

The problem of the non-universality of κ has been recently discussed in [44], who noted that the classical rationale for the log-law did not preclude κ depending on k^+. There are also several caveats to how flow data is processed to calculate κ, as recently discussed by Chen and García-Mayoral [50]. The requirement $\delta \gtrsim 30$–$40k$ is unfortunately too demanding for high-fidelity simulations, and is often not met in numerical studies. In fact, most of the studies cited above as observing values of κ significantly different from the smooth-wall value were conducted at lower δ-to-k ratio. Perhaps due to this, a best fit to a logarithm for the mean profile, typically obtained by setting its origin at a 'zero-plane displacement height', is often enforced in regions that include the roughness layer, where the flow should never be expected to be smooth-wall-like, or extending above the upper limit of the log layer, $y > 0.2$–0.3δ. Furthermore, the log layer is intrinsically an asymptotic concept for infinite scale separation between the inner and outer flow, which only occurs at infinite Reynolds

numbers. At finite Reynolds numbers, the mean velocity profile is never perfectly logarithmic, even over smooth walls, so enforcing a logarithmic behaviour is enforcing something that smooth-wall flows do not satisfy. This is easy to see in the 'diagnostic function', $y^+ \mathrm{d}U^+/\mathrm{d}y^+$, which would become constant and equal to $1/\kappa$ in the logarithmic region if the mean profile satisfied Equation (1) exactly. In practice, a plateau in the diagnostic function is only observed over smooth walls for $\mathrm{Re}_\tau \gtrsim 10{,}000$, which is beyond the current reach of rough-wall DNS.

Alternatively, [50] argued that outer layer similarity does not merely require the existence of a log layer that follows Equation (1), but rather that the whole flow sufficiently far from the wall be smooth-wall-like. This would also include the outer region, and this can be leveraged to extend the region where a collapse with smooth data is sought. Furthermore, they argued that, rather than agreement with Equation (1), what should be enforced is agreement with corresponding smooth-wall data at matching Re_τ, since the latter differs from an exact logarithm at any but the highest Reynolds numbers – for channel flow, $\mathrm{Re}_\tau \gtrsim 10{,}000$. They also noted that enforcing a match to a logarithm in some flow region without checking that the flow above matched smooth-wall data was at odds with full outer layer similarity. An example is shown in Figure 4. To check outer layer similarity, this example uses the diagnostic function, since it is more sensitive to deviations than the mean velocity profile. Due to its higher sensitivity, we advise to use the diagnostic function rather than the U profile to verify outer layer similarity. However, the differentiation required may make this function unsuitable if the U- and y-data is noisy, as is often the case both in experiments and simulations. In that case, a sensible alternative is to check for a constant offset in the velocity profile at all heights above the roughness sublayer, compared to corresponding smooth-wall data.

Figure 4 shows that displacing the origin so that the velocity profile matches a logarithm, or the diagnostic function exhibits a plateau, does not produce similarity with smooth wall data, whether the match is enforced within the expected bounds of the log layer or beyond. However, it is possible to enforce instead a collapse with smooth wall data, obtaining good agreement. For the example shown, a densely packed bed of elements, the resulting zero-plane displacement is then just below the roughness tips, instead of deep within the substrate, which is more consistent with the expected 'skimming' regime in a dense topology. More importantly, while enforcing a plateau in the diagnostic function resulted in a reported $\kappa \approx 0.32$ or even 0.28, enforcing full outer layer similarity resulted in a smooth-wall-like $\kappa \approx 0.39$.

The methodology described above was tested for a broad variety of substrate densities in [50], and it was found that a decrease in the value of κ was still observed for the most intrusive surface topologies. Nevertheless, this decrease was never larger than $\sim 15\%$, while those reported in the literature using log-matching can be as large as $\sim 50\%$. This suggests that the breakdown of outer layer similarity and departure from smooth-wall values of κ reported in the literature may need to be reassessed carefully. In any event, it remains to be verified if these deviations in κ occur only at small δ-to-k ratios. The simulations in [50] did not always satisfy the condition that the roughness layer does not protrude beyond 0.1δ as discussed above. Due to practical limitations, this is often the case for fully resolved simulations, which are frequently conducted at $\delta \approx 10k$. The comparison with simulations at larger δ-to-k ratio, e.g. in [50,51], suggests that $\delta \approx 10k$ is probably sufficient to study the alteration of inner and roughness layer dynamics, as well as changes to skin friction,

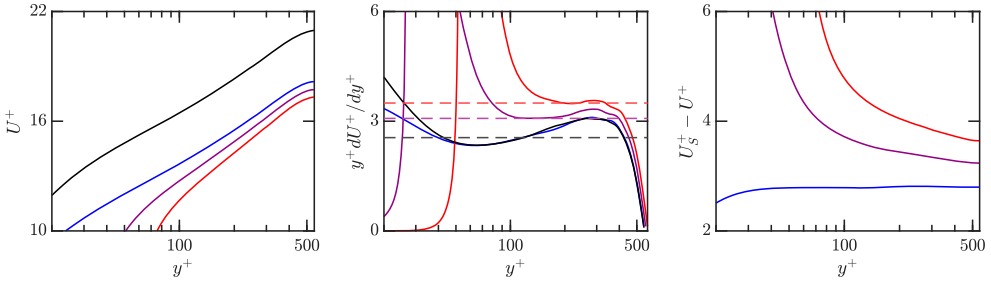

Figure 4. Mean velocity profile U^+, diagnostic function $y^+ \mathrm{d}U^+/\mathrm{d}y^+$, and mean-velocity difference with a smooth-wall flow $U_S^+ - U^+$, for the flow over a dense-canopy roughness, adapted from [50]. ——, reference smooth-wall flow at the same $\mathrm{Re}_\tau \approx 550$; ——, with y-origin shifted to maximise the depth of the region with a plateau in the diagnostic function; ——, with y-origin shifted to obtain a plateau only below 0.3δ; ——, with y-origin shifted to match the reference smooth-wall data. The dashed lines indicate the respective estimates for $1/\kappa$, corresponding to $\kappa \approx 0.28$, 0.32 and 0.39.

even if it may not be sufficient to determine conclusively the effect on the overlying log layer and the outer flow above, including on outer layer similarity and universality or not of κ, for which $\delta \gtrsim 30$–$40k$ would be necessary.

3. Surface roughness in non-equilibrium conditions

Concepts such as the roughness function or the equivalent sand-grain roughness rely on the assumption that the effect of the texture is confined to the near-wall flow, i.e. are developed under the assumption of outer-layer similarity [5]. Whether or not such characterisation of roughness applies under non-equilibrium conditions, when similarity breaks down and a conventional logarithmic layer may cease to exist, is an open question. Another objective of ongoing investigations is the downstream propagation of the effect of surface roughness, and how history effects accumulate and can be accounted for in models.

3.1. Roughness under pressure gradients

The work and findings of AVT-349 on the interaction of surface roughness and pressure gradients are discussed extensively in [14]. The conclusions and findings are briefly summarised here. In general, rough-wall flows exhibited Reynolds-number independence in outer units, at least for fully rough conditions, for a variety of pressure gradients. For favourable-pressure-gradient (FPG) flows, Townsend's outer layer similarity between rough- and smooth-wall boundary layers appears to largely hold, with rough-wall flows seeming to reach equilibrium more quickly following changes in the pressure gradient. Cases with strong enough FPG to cause relaminarisation on smooth walls have not been studied extensively with rough walls, although some numerical results are discussed below. Volino et al. [14] hypothesises that having k change depending on the local pressure gradient such that δ/k was constant for FPG, ZPG, and APG boundary layers would result in an 'equilibrium' roughness, and recommended that such surfaces be designed and studied under various pressure gradients to separate the effects of variable δ/k from other parameters. In any event, the conditions for similarity between rough- and smooth-wall boundary layers under pressure gradients need yet to be determined. The evidence discussed in [14] suggests that matching the history of the freestream velocity does not result in similarity for APG flows, but that similarity may be achieved if the history of β is matched. This supports future efforts, experimental and computational, to study flows with different freestream velocity evolutions but such that the histories of β are matched. This should include equilibrium flows, with constant β, and non-equilibrium flows with increasing β, as well as flows on the verge of separation.

Boundary-layer flows over rough surfaces were also studied numerically by Piomelli and co-workers [52–54]. Roughness was found to prevent the quasi-laminarisation of a boundary layer in strong FPG, and to accelerate separation in APG flows. In an FPG flow the log-law slope and intercept changed significantly in the FPG region. However Yuan and Piomelli [53] found that when the intercept was corrected using the relationship between k_s^+ and ΔU^+ valid for ZPG boundary layers it matched the smooth-wall value, suggesting that the equilibrium relationship may be relatively robust. Since these calculations considered a single pressure gradient, Reynolds number, and surface geometry, additional experiments and/or calculations would be desirable to extend this observation to other cases.

3.2. Surface heterogeneity

Rapid changes in surface roughness can cause severe departures from equilibrium conditions. Abrupt changes in the streamwise direction, such as smooth-to-rough and rough-to-smooth transitions, lead to sudden changes in the local friction that the flow needs to adapt to. Spanwise heterogeneity, in turn, leads to the appearance of large-scale secondary motions typically in the form of streamwise-aligned rollers. In applications, changes in roughness are not streamwise- nor spanwise-aligned, and so oblique changes, which can be viewed as a combination of streamwise and spanwise changes, ought to also receive our attention, as data is currently lacking [55].

In the case of abrupt rough-to-smooth changes, equilibrium modelling can lead to significant errors in the prediction of drag several boundary-layer-thicknesses downstream of the roughness change [56]. This

means, for example, that patches of roughness (such as those that occur on bio-fouled surfaces or in atmospheric boundary layers) are a challenge for prediction. Modelling errors can come from two main causes: the assumption of equilibrium on which many models are based and the fact that in many cases the perturbation starts at the wall and propagates outward. The assumption of equilibrium of the wall shear stress affects not only wall-modelled LES (WMLES) but also experiments that cannot access the viscous region, e.g. Preston tubes and Clauser charts [56]. Unlike the outer part of the boundary layer in WMLES, this non-equilibrium of the near-wall region is difficult to resolve, other than by direct simulation, and thus needs to be modelled [57].

Turbulence is out of equilibrium, for instance, in the case of the flow over spanwise-oriented roughness strips, a case that has been widely studied experimentally and numerically [56,59,60]. At the beginning of a rough strip the skin-friction increases well above the equilibrium value, due to the presence of a stagnation region at the leading edge of the rough strip. When the roughness height decreases, on the other hand, the roughness elements shelter the surface with lower roughness, leading to a decrease of the wall stress below the equilibrium value. Recent data show that the wall shear stress recovery is quicker than previously thought, even as non-equilibrium persists [61–63], and small scales nearer to the wall recover first [56,64]. A simple, simulation-free approach to model the effect is by retaining some upstream information through a blending model [58,64], originally proposed by Chamorro and Porté-Agel [65] and illustrated in Figure 5. The model can reproduce the depressed log-layer offset characteristic of this non-equilibrium flow that is not unlike that seen in some adverse pressure gradient or decelerated flows. The active terms in the mean-momentum balance are not the mean pressure gradient nor the mean advection but the balance between the viscous and altered Reynolds shear stress [66]. The depressed log-layer offset is then entirely described by $\partial\tau/\partial y \approx 0$ below $y^+ \lesssim 30$, where the total stress is defined by $\tau \equiv \mu\partial U/\partial y - \rho\overline{uv}$. This may, at first glance, suggest an equilibrium wall-modelling approach [57]. However, unlike equilibrium approaches where the damped eddy-viscosity $-\overline{uv} = (\kappa y[1 - \exp(-yu_\tau/\nu/A)]\partial U/\partial y)^2$ works well with a universal smooth-wall damping constant $A \approx 26$ [67], A is not universal after the rough-to-smooth transition, even after experiencing a smooth-wall fetch of one outer-layer height [66]. A similar phenomenon has been discussed in the context of wavy walls [68–70]. Because the dynamics are traced to the viscous region so close to the wall, it is unlikely that we will be able to resolve them even partially, leaving the burden of prediction on models in the foreseeable future.

For wall-modelled simulations, the fact that the recovery is not instantaneous causes models that use wall quantities to determine the eddy viscosity (the Spalart-Allmaras model in all its varieties, for instance) to predict the incorrect recovery of the wall stress [71]. Figure 6 shows a comparison of various models applied to a sequence of smooth and rough strips, similar to the configurations studied experimentally by Antonia and Luxton [59,60] or [72]. Two equilibrium models were used. The first one (EQWM), based on the assumption of an Equilibrium-Stress-Layer (ESL) model, is equivalent to imposition of the log-law; the Modified Moody diagram [73] calculates the wall stress using by interpolating the results of a numerical integration of the ESL equation. The IDDES model [74] is a variant of the DES approach that solves a transport equation for the eddy viscosity. Finally, the LaRTE model [75,76] is a model that solves a PDE for the friction velocity containing a term that represents the relaxation towards equilibrium that follows the imposition of a perturbation on the

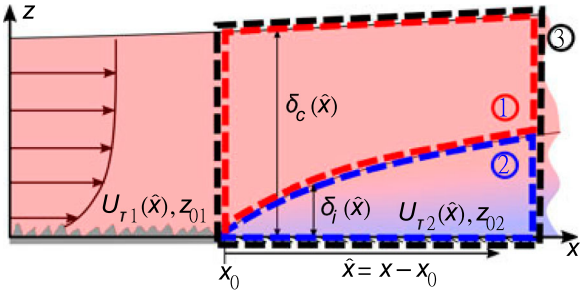

Figure 5. Schematic of the blending model for surface heterogeneity, taken from [58]. Downstream of a surface-topology sudden transition, the boundary layer has an upper region (1) still unaffected by the changes in the surface, which is essentially in equilibrium with the upstream conditions, and an internal boundary layer (2) where the information on the surface change is propagating and blending with the region above.

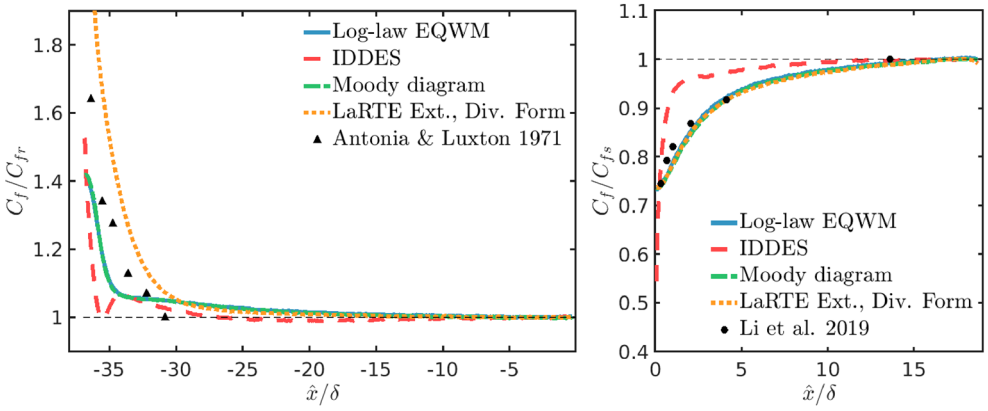

Figure 6. Skin-friction coefficient over spanwise-oriented smooth and rough-wall strips, normalised by the rough-wall and smooth-wall values. Adapted from [71].

wall stress. The models based on the ESL have a built-in memory of the state of the flow before the rough-to-smooth (or smooth-to-rough) transition, due to the fact that the velocity fed to the ESL is measured a certain distance from the wall, and is, therefore, unaffected by the transition for some distance. The IDDES model, which explicitly includes non-equilibrium effects, adjust too fast, as the eddy viscosity boundary condition is discontinuous. The LaRTE model is the one that gives the best agreement with the data, indicating that some memory effects must be retained. This is the approach followed also by Chamorro and Porte-Agel [65] and also discussed by Li et al. [58,64].

One of the shortcomings of wall-layer models is the weak, one-way, coupling assumed between the outer-layer LES and the near-wall region. In some cases (such as those discussed above) the perturbation propagating from the wall can still be predicted accurately. In others the near-wall phenomena cannot be modelled accurately, and errors propagate to the outer layer. A case in point is the flow over streamwise-oriented roughness strips. Nonlinear eddy-viscosity RANS closures, LES and DNS can all reproduce features such as the secondary flows seen over spanwise changes in roughness. However, the changes can be subtle [77,78]. In this particular flow configuration an imbalance in the viscous dissipation between the rough and smooth strips causes a spanwise velocity [79], and results in longitudinal vortices that affect the mean velocity profile by advecting slow fluid to the outer layer on the smooth strips, and fast fluids towards the wall on the rough sections of the wall. This is particularly difficult to predict in WMLES because the dissipation is maximum near the wall, well below the inner/outer layer interface, where the dissipation levels are much lower. As a consequence the longitudinal vortices predicted by WMLES are too weak, and the velocity deficit on the smooth-wall strips is underpredicted.

Possible ways to improve the results of WMLES include devising stronger coupling between inner and outer layer (but note that the IDDES approach gave the least accurate results in the spanwise-strips case), and by including a more physical description of the wall eddies near the Inner/Outer layer interface, where they are typically less active than in reality. The use of resolvent analysis [80,81] to generate synthetic turbulent eddies in the wall layer is under investigation; a WMLES in which the wall layer is populated by synthetic eddies may be able to capture extreme events and non-equilibrium effects better, and improve the coupling between inner-layer model and outer-layer LES. Ongoing work using resolvent analysis [80] shows promise for modelling secondary (wake) flows associated with wall roughness and has the potential of encoding history effects into wall models.

4. Effects of pressure gradients and non-equilibrium on smooth-wall turbulent-boundary-layer flows

The terms equilibrium and non-equilibrium of turbulent flows are not used in a unique sense in the literature, as pointed out in [82,83], and a short review is worthwhile before presenting the findings of the AVT-349.

Perhaps, the most common understanding of equilibrium in boundary layers is that of Clauser. Clauser used the term ‘equilibrium boundary layer’ to describe the existence of a self-similar solution of a TBL. The

conditions for self similarity were a balance between the different terms in the mean momentum equation (see [84]), in analogy to the Falkner-Skan laminar case. Clauser assumed a self-similar solution of the Reynolds shear stress (this is still subject to debate (see [85])) and a negligible role of the contribution from the streamwise gradient of the normal Reynolds stresses.

The argument by Clauser takes into account the role of the Reynolds stresses in the mean momentum balance, but not vice versa. However, the Reynolds stresses are governed by transport equations, which involve the local mean velocity gradients. This brings into focus the question of a balance between the relevant terms in the Reynolds stress transport equations. The relative magnitude of the tensors describing production P_{ij}, redistribution (pressure-strain) Π_{ij}, and dissipation ϵ_{ij} needs to be considered to discuss an equilibrium state of the Reynolds stress tensor at high Reynolds numbers (assuming the notion that the transport due to turbulent and pressure fluctuations loses importance for high Re (see [86])). Such a discussion of equilibrium from a viewpoint of the Reynolds stress budget seems to be missing in the literature (see [82]). This complete equilibrium might only be achieved in homogeneous turbulence, where the mean velocity gradients are constant. That case is described in the literature as 'moving equilibrium'. We note however that the term 'moving-equilibrium' is used in a different sense by Kader and Yaglom [87]. In their work, a boundary-layer flow is in moving equilibrium if the free-stream velocity U_∞ and the kinematic pressure gradient $(1/\rho)\mathrm{d}P/\mathrm{d}s$ are varying only slowly with the streamwise coordinate s so that the boundary layer adjusts to these variations and its structure at any value of s depends essentially on the relevant local parameters at the same streamwise position only, not on the upstream history of the flow.

Another use of the term 'equilibrium' is associated with flow regions in which production of turbulent kinetic energy P_k is equal to dissipation ϵ (see [82]). Related arguments have been used to design RANS models to account for the log law in turbulent boundary layer flows at zero pressure gradient (as described in [88]). However, in order to achieve a self-similar solution of the Reynolds shear stress, a (near-)equilibrium state of anisotropies of the Reynolds stresses might be needed, which does not necessarily follow from $P_k = \epsilon$. As described in [89], taking the trace of the balance $0 = P_{ij} + \Pi_{ij} - \epsilon_{ij}$ and assuming incompressible flow yields $P_k = \epsilon$. The opposite direction is more complicated, since physically the unclosed pressure-strain tensor is not a local function of the mean velocity gradient and the Reynolds stress anisotropy. In contrast, within the framework of RANS turbulence modelling, if such a local dependency for the pressure-strain tensor is assumed, then it can be shown that the anisotropy of the Reynolds stresses is determined by the calibration of the model for the pressure-strain term (see [89]). On the other hand, flows with production exceeding dissipation like homogeneous shear flows (with P_k/ϵ in a constant ratio once the flow is mature) are supposed to exhibit an (approximative) equilibrium state in the sense of constant Reynolds stress anisotropies (see [90]) and self-similar mean velocity profiles. The same applies to the mixing layer. Hence, flows with a constant ratio of P_k/ϵ different from one are not necessarily complicated nor do they preclude a self similar solution (see [88,91]).

In the present work, the term non-equilibrium is used loosely to mean local rapid changes of the flow in the streamwise (and, in 3D flow, in the lateral) direction over a distance which is sufficiently small relative to the boundary layer thickness δ. One could imagine that, for sufficiently rapid changes of the streamwise (and possibly, the lateral) pressure gradient, the induced changes in the mean velocity gradients could cause a local disturbance in the balance between production, pressure-strain and dissipation. Then, the Reynolds stress anisotropies could also change in the streamwise direction. In either case, such a situation would imply that the different terms of the mean momentum equation are unbalanced, or in other words much more dynamic, and a self-similar solution cannot form.

4.1. Non-equilibrium flow conditions and similarity

Under AVT-349, three different types of non-equilibrium flows have been investigated. The first type had a streamwise changing pressure gradient, from favourable to adverse, or, vice versa, from adverse to favourable. This has been studied in the two-dimensional boundary layer flow experiments by Virginia Tech. The change from FPG to APG has also been studied in the experiments by the US Naval Academy and by DLR/UniBw. The second type of flow was the relaxation of a turbulent boundary layer at ZPG after the removal of the APG (the flow in the APG region downstream of the ZPG region is of its own interest). This case was studied in the experiment by the University of New Hampshire (UNH). The third case considered the combined

effect of a streamwise changing pressure gradient, from favourable to strongly adverse, in conjunction with a mild convex surface curvature, and the relaxation from curvature on a flat plate. This was studied in the joint DLR/UniBw experiment, see [92].

One key question identified by the task group is whether similarity exists in non-equilibrium flows; and more specifically, whether concepts underpinned by outer-layer similarity in canonical frameworks are applicable in non-equilibrium flows. Following the classical work by Rotta [93] and Clauser [84], self-similarity of the mean velocity profile in the outer layer can be expected only in the case of equilibrium turbulent boundary layer flows. Then the pressure gradient parameter $\beta_{\mathrm{RC}} = \delta^*/\tau_w dP/dx$ needs to be constant in the streamwise direction. In a streamwise-evolving turbulent boundary-layer flow, the relative importance of the different terms of the mean momentum balance (pressure gradient, mean inertia, viscous stresses and Reynolds stresses) is changing in the streamwise direction, and hence β_{RC} is not constant. The question of outer-layer similarity in non-equilibrium flows is discussed in the companion paper [94] of this special issue.

The other key question is on similarity in the overlap layer. The log-law for the mean-velocity for smooth and rough surfaces is fundamental for the design of RANS turbulence models and for the calibration of classical near-wall models for LES, see [88,91] (note, however, that after being calibrated, the models can be used in flows without a log-layer). Determining the validity of the log-law in flows with significant pressure gradient and non-equilibrium conditions is of high importance and is still an open question in the research literature. The resilience of the log-law in turbulent boundary layers with pressure gradients near equilibrium is widely reported, e.g. in [95–97]; however, significant departures can be seen under strong pressure gradients, at laboratory Reynolds numbers [98]. Much less is known in flow regions with a significant deviation from equilibrium. An example is the flow in a suddenly highly accelerated turbulent boundary layer [99]. A combination of theoretical reasoning and RANS simulations was used by Spalart [100] to argue that the log-law can be altered by a sudden change of the wall-shear stress velocity u_τ over a short time. Note that the resilience of the log-law in adverse pressure gradients is also discussed, from a different perspective, in the contribution by Klewicki et al. [94] in this special issue.

4.2. Pressure gradient effects versus non-equilibrium effects

Non-equilibrium effects are not explicitly accounted for in RANS models, but models were found to be (to a certain degree) suitable to describe non-equilibrium flows in mild PG (e.g. the 2D Virginia Tech flow [101]), as described in [94] in this special issue. From the present data available, the first order history effects that need to be better modelled are not clear. This observation is in concurrence with the investigation of a large data base of equilibrium flows and non-equilibrium flows in [102].

Traditionally, the mean velocity is described by the law-of-the-wall/law-of-the-wake by Coles [95]. Some publications discuss a change of κ due to a significant PG, see [103,104]. Note that this topic is discussed in more detail in the companion paper [94] of this special issue. In the case that a change of κ is assumed/accepted, the question arises as to whether κ changes (i) due to a (strong) PG in near-equilibrium flows and/or (ii) due to non-equilibrium effects. A change of κ due to an APG was recently used to modify RANS models, see [105,106]. There are only few data for a strong APG, say, for $\Delta p_x^+ \geq 0.01$. A reduction of κ to 0.37 for $\Delta p_x^+ = 0.01$ is reported in [103]. On the other hand, the data suggest that κ does not change significantly in a mild/moderate APG, say, for $\Delta p_x^+ \leq 0.007$. In any case, one needs to be cautious, as changes of κ can be due to indirect effects, i.e. due to a low Reynolds number, as a clear log-law region is hardly seen at low Re due to the blending between inner and outer layer, and a plateau in the mean velocity slope diagnostic function is likely not found. Moreover, the influence of the measurement uncertainty (mainly of the friction velocity) on the value inferred for κ is significant (see [92]). On the other hand, non-equilibrium effects could lead to a variation of the apparent value for κ, as described above (see [100]). In the DLR/UniBw flow, a reduction of κ in the upstream region of a streamwise changing pressure gradient and convex curvature was observed, which could be the reason for a small reduction of κ found in the APG region downstream.

Another feature of a TBL at zero-pressure gradient is that the inertial sublayer can be associated with the log law in the mean velocity. In the traditional view, the log law is the overlap between inner and outer regions and is common to both. This is worth being studied for non-equilibrium pressure-gradient flows. The outer

edge of the log law at ZPG is, in good agreement, near 0.15δ. In strong APG, the outer edge of the log-law region was found to be no longer around 0.15δ. Instead, smaller values were found (see the investigation of a large data base of TBL flows in various APGs in [102]). Regarding the flows studied within this AVT, for the DLR/UniBw flow, the mean velocity profile for u^+ is found to turn above the log-law for around $y^+ > 0.05\delta^+$ in the strong APG region. While for the DLR/UniBw flow, the erosion of the log-law region already appears in the upstream region of favourable pressure gradient and convex surface curvature, a reduction of the outer edge of the log law is also found for flows near equilibrium in the absence of surface curvature, e.g. the flow by Skare and Krogstad and the University of New Hampshire flow (see [102]). It is not clear, if such a reduction of the outer edge of the log law (in ratio to δ) is an APG effect or a non-equilibrium effect. On the other hand, in FPG and weak/mild APG flows near equilibrium, the resilience of the log-law region in the mean velocity was found (within the experimental accuracy).

Regarding the resilience of the log law in FPG and in a mild APG, RANS modelling for flows with PG should account for this by ensuring that the log-law is not altered in the log-law region. Shielding of the log-law calibration of RANS might be needed, in particular, if machine-learning methods are used for a global modification of a RANS model.

Interestingly, for Couette-Poiseuille (CP) flow, studied by Telbany and Reynolds [107] and Nakabayashi et al. [108], such a systematic erosion of the logarithmic layer in the mean velocity is also reported. As CP flow is a self-similar flow in dynamic equilibrium in the sense of [109], this would indicate a progressive breakdown of the universal law of the wall as a consequence of the pressure gradient and not as a history effect. It is worthwhile mentioning that the progressive erosion of the log-law region was earlier reported by Kader and Yaglom [87] for a large number of turbulence boundary layer flows in an APG.

The question of a wall law for the mean velocity in the inner layer is traditionally related to the question of what is a sufficiently high Reynolds number. Figure 7 (left) shows the values for β_{RC} versus Re_θ for the flows studied within this AVT. Moreover, classical data from the literature collected in [95] and more recent experimental studies of TBLs in an APG are included. The figure legend uses the nomenclature by Coles and Hirst [95] and Knopp [102], including the numbers used as identifiers for each flow used by Coles and Hirst [95]. For the DLR/UniBw flow, the data for two Reynolds numbers, achieved at two different velocities, are shown.

The lack of data at high Reynolds numbers becomes obvious, in particular regarding naval applications. Full scale ship Reynolds numbers easily reach $Re_L = 10^9$ based on the length of the hull L. However, although $Re_\theta = 80{,}000$ is very high for wind-tunnel experiments, it corresponds to only $Re_L = 9.6 \times 10^7$, assuming $\theta/\delta_{99} = 1/8$ and $\delta_{99}/L = 1/150$ at full scale ship Re for the sake of simplicity.

The indication of an erosion of the log law region in strong APGs is illustrated in Figure 7 (right). The outer edge of the log-law region is denoted by $y_{log,max}$. In significant APG ($\beta_{RC} > 10$), $y_{log,max}/\delta$ is found to be smaller than the value of around 0.15 found for TBLs in ZPG and in mild APG. Regarding the DLR/UniBw flow, the figure suggests that significant upstream convex-curvature and non-equilibrium effects cause an additional reduction of $y_{log,max}/\delta$. Moreover, a different trend compared to the other flows is observed, viz.,

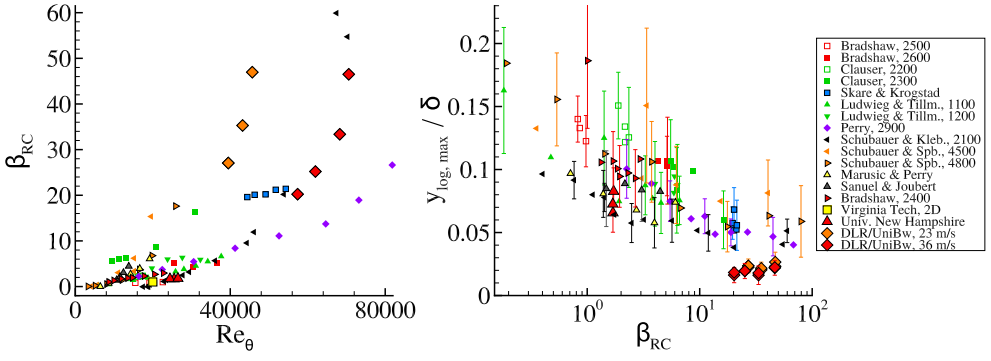

Figure 7. Left: Characterisation of APG flows studied in AVT-349 and data base from the literature. Right: Possible erosion of the log law region due to strong APG. Figures from [102] with small adjustment in the layout. The legend is taken from [95,102] using the numbers introduced by Coles and Hirst [95] as identifiers for each flow.

a mild increase of $y_{\log,\max}/\delta$ for increasing β_{RC}. This increase of $y_{\log,\max}/\delta$ might be due to an additional opposite effect beyond the APG, i.e. the recovery of the log law after the removal of convex curvature on a flat wall.

4.3. Modification of RANS models to account for effects of adverse pressure gradients

The effect of a strong pressure gradient on the law-of-the-wall/law-of-the-wake can be described by an increase in the wake factor Π (see [95] and the discussion in [83]). Several empirical correlations $\Pi(\beta)$ have been proposed (see [110]). The increase in the wake factor leads to a reduction of the log-law region. Alternatively, one might try to fit the mean velocity profile in the inner layer using some power law, inspired by the half power law proposed by Stratford for a zero-skin-friction flow. This brings up the old idea of a wall region by Perry [111] and Perry et al. [112], in which the mean velocity and the Reynolds shear stress is determined by local flow quantities, referred to as the 'local similarity hypothesis'. The question if a wall-region exists below the historical region in the outer part of the boundary layer is of high interest for RANS modelling. For the University of New Hampshire flow, distance-from-the-wall scaling was found in a moderate APG, see [94] for details; this could be interpreted as a linear variation of the mixing length. From this in conjunction with the appearance of a pressure contribution to the velocity scale, a power law region for the mean velocity could be inferred (see [113]), in concurrence with the proposal of a half-power law by Stratford [114] and Kader and Yaglom [87].

It has been shown in the literature, that the standard two-equations models (k-ϵ, k-ω) do not satisfy a half-power law solution (see [88]). There have been some attempts to modify RANS models to account for a half-power-law solution [106,115–117]. Such a half-power law (or a different power law) is still speculative, as convincing support from experimental data and/or DNS/LES is missing, and it is not clear to which extent it could serve as a useful modelling approach for engineering applications (similar to the log-law for the design of RANS models). A convincing support of a (half-) power law is expected to require high values of Re_τ and Δp_x^+ (see [87,94] in this special issue). Values of $\mathrm{Re}_\tau = u_\tau \delta/\nu > 2 \times 10^4$ and $\Delta p_x^+ > 0.01$ seem to be needed, as inferred from [102].

There are some indications that for flows in a strong APG close to equilibrium, RANS models cannot fully capture the effect of the pressure gradient. The equilibrium TBL at a strong APG of $\beta_{RC} = 20$ by Skare and Krogstad [118] was studied by Sporschill [106]. This revealed that even differential RSMs do not correctly predict the reduction of the mean velocity in the inertial sublayer (the inner part of the boundary layer) in a strong APG. A similar overprediction of the mean velocity in the inertial sublayer was found for the non-equilibrium DLR/UniBw flow (see [117]). The reduction of the mean velocity in the inner layer could be a first-order effect of the APG. (Concerning the DLR/UniBw flow, one should keep in mind, however, that there is an influence of the convex curvature non-equilibrium region upstream of the APG).

Regarding the conjecture of the existence of a (half-)power law region in the inner layer at a strong APG, Figure 8 (left) shows the mean velocity profile for u^+ versus $(y^+)^{0.5}$ for the DLR/UniBw flow (case $U_\infty = 36\,\mathrm{m/s}$) in the region of a strong APG. A region of a straight line would indicate a half-power law region (which is indicated by the two black vertical lines). The black dashed line gives the half-power law with $U(y) = 2/K((1/\rho)(\mathrm{d}P/\mathrm{d}s)y)^{0.5}$. Here s is the streamwise wall-tangential direction, P is the mean pressure, y is the wall distance, and K is sometimes called the Stratford constant, for which a value of 0.41 is used here. The slope of the mean velocity profile obtained by the original SSG/LRR-ω model is smaller than the half-power law would suggest. The modified SSG/LRR-ω yields a better agreement in the supposed half-power law region, and also for the skin friction coefficient.

4.4. Non-equilibrium effects and their modelling in the RANS framework

The response time of the mean flow to a streamwise change of the pressure gradient is expected to be varying in the different regions of the boundary layer. In this sense, the mean velocity profile at any streamwise position is the cumulative result of local conditions and historical effects [109]. As described in [119], the outer layer does not respond immediately to a change in $\mathrm{d}P/\mathrm{d}x$, whereas in the near wall region, velocity gradient and turbulent stresses are affected immediately. The concepts of the eddy-turn-over-time or lag between stress and rate of strain have been invoked to describe non-equilibrium response (see [120–122]). History effects

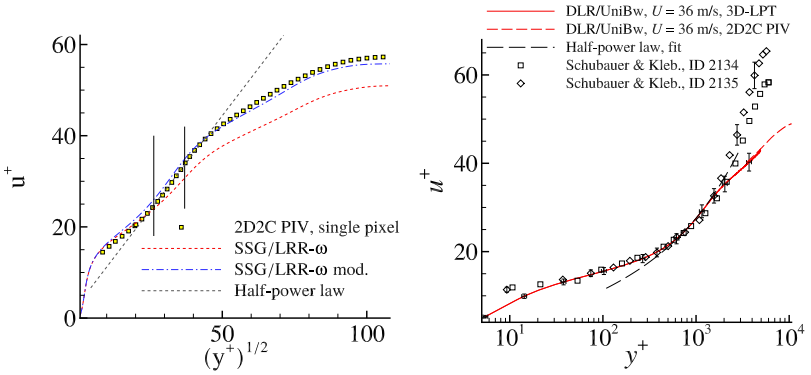

Figure 8. Left: Mean velocity profile for the DLR/UniBw flow at $\mathrm{Re}_\theta = 68{,}000$, $\Delta p_x^+ = 0.018$ plotted versus $\sqrt{y^+}$ (figure from [117]). Right: Non-equilibrium effects on the mean velocity profile for two flows (DLR/UniBw flow and Schubauer & Klebanoff) at similar values of the local boundary layer parameters $\mathrm{Re}_\theta = 57{,}000$, $\Delta p_x^+ = 0.01$ and $\Delta u_{\tau,x}^+$ but with a different pressure gradient history (figure from [92] with minor adjustments in the layout).

are expected to be stronger in the outer part of the boundary layer than in the inner layer. This is already known for turbulent boundary layer flows at ZPG, where perturbations in the outer part of the boundary layer were found to be long-lasting in downstream direction [123]. A transport equation model for accumulated history effects was devised by Smits et al. [121].

Figure 8 (right) is used to illustrate the conjecture that the mean flow in the inner layer could respond rapidly (although not instantaneously), whereas the response is significantly delayed in the outer layer. The figure shows the mean velocity profile for u^+ for the DLR/UniBw flow and for the turbulent-boundary-layer flow over a large airfoil-like body by Schubauer and Klebanoff [95]. In the latter case, the flow is first subjected to a significant favourable pressure gradient (FPG) in the nose region of the body over a streamwise distance of around 7 ft, followed by a mild FPG over a length of 11 ft, and then enters into a 8 ft-long region of APG and convex-surface curvature. The two flows differ in the details of streamwise-pressure-gradient history and surface curvature. The local boundary layer parameter are similar at the streamwise positions used in this plot. For all profiles, Re_θ is around 57,000, the pressure gradient parameter in inner viscous scaling Δp_s^+ is around 0.011 and in Rotta-Clauser scaling β_{RC} around 26, and the local streamwise acceleration parameter in viscous units $\Delta u_{\tau,s}^+ = \nu/u_\tau^2(\mathrm{d}u_\tau/\mathrm{d}s)$ has similar values. The uncertainty due to the method used to determine the wall shear stress is included, and one should be cautious to draw definite conclusions. However, it is of interest to see that the inner layer solutions are surprisingly close to each other. The mean velocity profiles for both flows exhibit the resilience of the log law. Above the log law, the mean velocity profile can be fitted by a half-power law in a certain part of the inner layer. These observations could indicate the role of local effects and the rapid response of the inner layer. On the other hand, the differences in the outer layer are due to the different flow history and can be clearly seen. For more details, see [92].

The time scale(s) of the delayed response of mean-flow and turbulence statistics to a non-equilibrium flow situation (in the sense of a sudden change in the boundary conditions, e.g. a streamwise changing pressure gradient or a change in surface roughness) and their descriptive modelling requires further investigation. The relative orientation of the Reynolds stress tensor to the local mean strain rate tensor can change, and in some situations the Reynolds stresses are found to lag behind the mean shear rate tensor [88]. For RANS models based on the Boussinesq hypothesis, stress-strain misalignment in non-equilibrium turbulent flows was accounted for in lag models devised by Olsen and Lillard [124] (see also [125]). A more complex model for replacing the turbulent-viscosity hypothesis with a non-equilibrium closure was proposed by Hamlington and Ihme [126]. Another aspect is that the response could depend on whether a pressure gradient is imposed, or if relaxation from a pressure gradient occurs. Non-equilibrium flows could give an opportunity for Reynolds stress transport models to show their potential advantage over linear eddy viscosity models. Rapid-distortion theory is expected to be a useful approach only during the initial response, but is not expected to describe the whole response process, including the long relaxation phase [119].

4.5. Possible paths for non-equilibrium turbulent boundary layer flows

Concerning future paths for the improvement of RANS turbulence models for smooth-wall non-equilibrium turbulent boundary layer flows, the findings from the two-dimensional smooth wall flows by Virginia Tech and DLR/UniBw within this project give good reasons to advocate following two routes. The first route is to further study the isolated effect of a pressure gradient on turbulent boundary layer flows near equilibrium. The second route is the investigation of non-equilibrium pressure gradient effects.

4.5.1. Flows near equilibrium in a significant pressure gradient

There are still many open questions associated with turbulent boundary layer flows near equilibrium in a significant pressure gradient. Both adverse and favourable pressure gradient cases are of high interest. For the validation and for the improvement of RANS turbulence models, new experimental data from wind-tunnel campaigns are needed. There is still a lack of test cases at high Reynolds numbers (see [102]), in particular for strong APG. Moreover, complementary data from DNS/LES are of high interest for modelling, as all terms of the budget of the Reynolds stress equation as well as very accurate data for the wall shear stress are obtained. However, currently it is impossible to do this for the target high Reynolds numbers applicable to full-scale aircraft and ship operations. The recent work by Eça et al. [127], published as output of AVT-349, suggests that at full-scale Reynolds numbers, the effect of turbulence modelling details are less pronounced than at model scale, and so more information on Reynolds stress details coming from model-scale DNS/LES could be helpful to better predict full-scale flows with pressure gradients (see also [128] in this special issue).

Concerning APG flow, what is needed to shed more light on the resilience and on the erosion of the log law are additional data involving a systematic variation of the overall effect of the PG (associated with $\beta_{\mathrm{RC}} = (\delta^*/\tau_{\mathrm{w}})(\mathrm{d}P/\mathrm{d}x)$), the local Reynolds numbers $\mathrm{Re}_\tau = u_\tau \delta/\nu$ and $\mathrm{Re}_\theta = U_\mathrm{e}\theta/\nu$ (U_e being the boundary layer edge velocity and θ being the momentum thickness), and the pressure gradient parameter in the inner layer $\Delta p_x^+ = \nu/(\rho u_\tau^3)(\mathrm{d}P/\mathrm{d}x)$.

For strong favourable pressure gradients (FPGs), much less is known. The number of data sets from experiments and DNS/LES is much smaller compared to APG flows. For strong FPG, the phenomenon of relaminarisation was observed at model-scale Reynolds numbers. The role of Reynolds-number effects on relaminarisation has not been studied in the literature, and little can be said about the relevance of relaminarisation for naval flows at ship-scale Reynolds numbers. Traditionally, relaminarisation is correlated with the acceleration parameter $K = (\nu/U_e^2)(\mathrm{d}U_e/\mathrm{d}x)$ exceeding a threshold value of around 3.5×10^6, see e.g. [129,130]. Here U_e denotes the boundary-layer-edge velocity. Note that K can be written as $K = Re_{\delta^*}^{-1}(C_f/2)\beta_{\mathrm{RC}}$ and therefore, if expressed in terms of β_{RC}, a dependence of the Reynolds number can be revealed which has not been explored yet. Moreover, in the case of surface roughness, it may be even more difficult to get relaminarisation. Beyond the topic of relaminarisation, there is a need for turbulent flows in a significant FPG (well below relaminarisation) at high Reynolds numbers, as the recent experimental investigations were performed at moderate Reynolds numbers [104,131]. Here, it is worthwhile mentioning that the definition of high and moderate seems to be depending on author/reader and is not specified in the literature with consensus in the community.

4.5.2. Non-equilibrium flows in a significant pressure gradient

Much less is known for non-equilibrium flows in a significant pressure gradient. Besides the cases studied in this initiative, the effect of the upstream history on the mean velocity profile and on the Reynolds stresses was recently demonstrated in several studies [132–134]. The available test cases appear as isolated islands in the landscape of a much larger parameter space. The parameter space and its dimensions are not clear at present. A combination of theoretical analysis and empirical findings could be a first step to identify parameters which characterise the departure from equilibrium and paths from and return to equilibrium.

In a first step, such a characterisation could employ a suitable parametrisation of the strength of the pressure gradient as well as parametrisation of the streamwise distance over which a pressure gradient is changing (probably related to the boundary layer thickness). Such a parametrisation could lead to a new series of parametric experiments performed in a wind-tunnel or another experimental facility (with maybe more favourable flow features for a specific application, such as the absence of the background pressure gradient due to the built-up of the boundary layers at the walls of the tunnel, e.g. by using a towing tank) or via DNS/LES.

For illustration, imagine the following extension of the 2D VT experiment (which is described in [94] in this special issue): the boundary layer thickness at the beginning of the non-equilibrium region could be varied by altering the streamwise position of the 2D airfoil; the streamwise distance over which the pressure gradient is changing could be altered by varying the airfoil chord length; and the strength of the pressure gradient could be varied additionally by changing the distance of the airfoil from the wind tunnel wall.

The following different types of flow history due to a streamwise changing pressure gradient arise. On the one hand, the flow can involve either only an APG region or a FPG region. Pure APG flow ($dC_p/dx > 0$) can be in increasing APG ($d^2C_p/dx^2 > 0$) (see e.g.[135]) or in decreasing APG ($d^2C_p/dx^2 < 0$) (studied, e.g. by Perry [111]). Similarly, a pure FPG flow can be in increasing or decreasing FPG. On the other hand, there is the situation of relaxation from APG or from FPG in a ZPG (after removal of the pressure gradient). A test case involving relaxation from FPG at ZPG is missing in the literature. Finally, flows can involve a streamwise changing pressure gradient from ZPG to APG and then to FPG (ZPG-APG-FPG), or from ZPG to FPG and then to APG (ZPG-FPG-APG). This is what happens for example near the bow and the stern of a ship or the nose and the trailing edge of an aircraft wing.

It should also be mentioned that in many applications (manoeuvring naval craft, for instance) the pressure gradient does not evolve in space only, but also in time. This may result in a large-scale unsteadiness of the separation, for instance, which is forced by the time-varying pressure gradient, but not necessarily synchronised with the forcing. The ratio between the forcing period and the flow timescale is an important parameter, that may result in very different physical phenomena. Recent wall-resolved LES by Ambrogi et al. [136,137] discuss this phenomenon. The high-fidelity data generated by these simulations was then used to evaluate turbulence models for the RANS equations by McDougall et al. [138]. The RANS simulations used the same numerical scheme and boundary conditions as the LES, and a mesh on which mesh convergence was achieved for the LES. The criterion for grid convergence of the LES was to ensure that the differences in the mean velocity between the final two grids were below 2%. The time step was adjusted to maintain a CFL number below 0.6 everywhere in the flow. By using these criteria, Ambrogi et al. could isolate the modelling errors from those due to numerics or boundary conditions. As a comment, regarding the scope of the present work, it would be interesting to quantify the uncertainty due to the spatial and temporal discretisation error following the guidelines by Eça et al. [139]. Note that the companion paper by Knopp et al. [128] in this special issue is dedicated to the topic of errors and uncertainties in CFD validation. On the other hand, regarding the time-discretisation error, using the LES time step is expected to yield a sufficiently small time-discretisation error when used for a (U)RANS simulation. The same is expected when using an LES mesh regarding the spatial discretisation error of a (U)RANS simulation.

All RANS models performed surprisingly well. They were able to predict the shedding of the recirculating region that is also observed in pitching airfoils when the ratio of timescale is approximately one. The skin-friction coefficient and mean velocity profiles were also in fair agreement with the data. Integral quantities such as the lift were also accurately predicted. This study uses a grid that is much finer than those expected in RANS, very clean numerics, a time-step size for LES resolution, and precisely defined boundary conditions. In real applications additional uncertainties due to these effects would likely decrease the accuracy of the calculations. However, they point out that often errors that are attributed to the turbulence models are in fact due to other causes, and suggests that overly pessimistic conclusions may be reached when comparing RANS results with simulation or experimental data.

Regarding rapid changes of the pressure gradient in space, the flows studied within AVT-349 cover some of the above situations. The flow by the University of New Hampshire (UNH) and by DLR have a streamwise changing PG. The UNH flow involves relaxation from APG, whereas the DLR/UniBw flow is in a streamwise decreasing APG. It is of interest to mention, that the relaxation of a TBL from convex curvature was studied in [140]. The 2D Virginia Tech flow studies the streamwise change ZPG-APG-FPG and ZPG-FPG-APG.

Since the work of Stratford [114], the relevance of d^2C_p/dx^2 for the largest possible increase in C_p that a TBL can sustain without separation, is known. Early experimental investigations studied the effect of d^2C_p/dx^2 [111,135]. These classical studies and considerations are worth being revisited for the design of new non-equilibrium experiments.

The topic of flow non-equilibrium deserves also a study of the budget of the Reynolds stress equations. This can be achieved with a sufficient accuracy at present only from DNS results, as the pressure-strain tensor can

hardly be obtained from experimental data. It is expected that a deepened understanding of non-equilibrium flows can be accomplished only by complementary DNS data.

To summarise, new wind-tunnel experiments imposing families of streamwise pressure gradient distributions as used in [101,141] in conjunction with DNS efforts are suggested to foster the progress in RANS turbulence modelling for non-equilibrium turbulent boundary layer flows.

4.5.3. Potential for improvement of RANS turbulence models

RANS turbulence models based on transport equations for turbulence quantities can in principle account for (some) history effects, and are expected to be less limited than algebraic turbulence models. Some modelling assumptions reduce the ability to account for non-equilibrium effects. The turbulent viscosity hypothesis relates the Reynolds stresses in the mean momentum equation to the local strain rate tensor, which is a significant simplification. Therefore model improvements of eddy-viscosity RANS turbulence models to account for non-equilibrium effects might need to start from a lag extension ([124,125]). Differential Reynolds stress models (DRSM) could exhibit their potential for non-equilibrium flows.

For the calibration of RANS models, the assumption of a fixed ratio (not necessarily unity) of production of turbulent kinetic energy (TKE) and dissipation is used. For the log-law region at ZPG, the ratio is unity. The question as to whether this needs to be extended for flows departing from equilibrium is still open. Another open issue is as to whether the anisotropies of the Reynolds stress tensor change from their (approximative) values in equilibrium turbulent boundary layer flows. Such a deviation might depend on the strength of the departure from equilibrium. DRSM can, in principle, predict a time evolution of the Reynolds stress anisotropy. E.g. for homogeneous, parallel shear flow, the time evolution of the anisotropy tensor starting from isotropic turbulence to an anisotropic equilibrium state can be described, and the time scale is of order k/ϵ (see [88]). Another question is about the trajectory within the anisotropy invariant triangle (sometimes referred to as the Lumley triangle) during departure from and return to an equilibrium state. It is not clear if this improves the overall predictive accuracy of the model.

Transport-equation-based RANS turbulence models involve different terms and quantities, which involve mechanisms to account for non-equilibrium effects. In two-equation RANS models, the transport equation for ϵ (or ω) provides a mechanism for the turbulence frequency $\omega = 1/T$ (using the turbulence time scale $T = k/\epsilon$) to relax towards an equilibrium value S/β, which is taken from the time scale of the mean strain rate S and an empirical constant β (β is known to be different for wall bounded flows and free shear flows) [142]. In differential Reynolds stress models, the turbulence time scale is used in the model for the slow part of the pressure strain correlation model describing the redistribution of Reynolds stresses (see [88]). It is not clear whether or not a single time scale is sufficient and if the turbulence time scale $T = k/\epsilon$ is the most appropriate choice. A limitation in predicting non-equilibrium effects might be due to a single turbulence time scale. A review of the concept of a multiple scale model proposed by Gleize et al. [143] could be worthwhile.

A series of closures for the Reynolds stress anisotropy and a final modified constitutive relation were proposed in [126] to describe the response of homogeneous turbulence to rapid changes in mean shear. As described above, rapid-distortion theory is an applicable approach only during the initial response, but is not expected to describe the whole response process (see [119]). On the other hand, the ideas and techniques used in this work might be worth being revisited and could lead to non-equilibrium modifications in other places in the turbulence model closure assumptions.

4.6. Data-driven models

Performing high-fidelity (i.e. DNS or wall-resolved LES) analysis of non-equilibrium turbulent flows, in particular statistically three-dimensional and adverse pressure gradient flows, remains too computationally costly, in particular for design iterations and/or full-scale applications, and therefore modelling is required. Reynolds-Averaged Navier–Stokes (RANS) approaches based on a linear Boussinesq approximation still represent the standard for many industrial applications as they usually offer a reasonable trade-off between time-to-solution and accuracy. However, these models have been established and calibrated mainly for statistically two-dimensional equilibrium flows and therefore cannot be guaranteed to satisfactorily represent non-equilibrium effects. To address some of the weaknesses of linear RANS models, several evolutions have

been proposed, such as Explicit Algebraic Reynolds Stress Models (EARSM), which invoke a weak equilibrium hypothesis [144] to expand the anisotropy tensor in terms of a tensor basis and scalar invariants [145] and add the non-linear terms to the linear Boussinesq approximation as:

$$\overline{u_i u_j} = \underbrace{\frac{2}{3}k\delta_{ij}}_{\text{isotropic}} - \underbrace{2\nu_T S_{ij}}_{\text{lin. Boussinesq}} + \underbrace{2k\sum_{n=1}^{10}\xi_n T_{ij}^{[n]}}_{\text{extra anisotropy}} \tag{3}$$

Thus, the Reynolds stress $\overline{u_i u_j}$ is related to its trace $2k$, strain rate tensor S_{ij} and a linear combination of basis functions $T_{ij}^{[n]}$ [145], formed from polynomials of non-dimensional strain $s_{ij} = \tau S_{ij}$ and rotation rate $\omega_{ij} = \tau \Omega_{ij}$, with τ being the turbulence model timescale. The coefficients ξ_n in Equation (3) are functions of the non-dimensional invariants I_n produced from s_{ij} and ω_{ij}, of which there are five for three-dimensional flows [145]. Following [146], a second model can be developed to correct the production term in k-ω turbulence transport equations. The turbulence production correction term is modelled as $R = 2k\hat{R}_{ij}\frac{\partial u_i}{\partial x_j}$.

Thus, the modelling problem is transferred to finding the coefficients ξ_n in front of each tensor basis term. This has in the past been achieved with human intelligence, such as in [147,148]. This task, however, can also be effectively addressed by emerging machine-learning technologies that can be exploited for their capability of approximating complex functional relationships between inputs and outputs. Therefore, an increasing number of machine learning and deep learning methods have been employed for data-driven turbulence model training [149–152].

In recent symposia on turbulence modelling [153,154], a list of challenges, recommendations and *desiderata* was proposed. The emerging and promising role of machine learning data-driven technologies was acknowledged. A debated aspect was the possibility of developing a 'universal' turbulent closure model where the universality should be related to the capability of making improvements in at least some key areas while doing no harm in others. Model interpretability, data consistency, features importance and sensitivity, extrapolation detection, were other elements recognised to be critical to approach this challenging task.

Irrespective of the data-driven methodology employed to develop a closure, a pivotal difference lies in the machine-learned models' ability to exhibit efficacy in either *a priori* or *a posteriori* validation. In the former, a trained model is employed to approximate training or alternative test datasets, using as inputs the testing data. Conversely, in the latter, the data-driven models are incorporated into a flow solver and subjected to assessment through computational fluid dynamics (CFD) evaluations, crucially thereby using the CFD-predicted fields as inputs. Closures performing well in this mode are deemed 'model-consistent'.

For modelling activities within the AVT-349 program, we have used Gene Expression Programming (GEP) [155,156], a symbolic regression technique based on evolutionary algorithms, which produces models that are interpretable and allow for straightforward implementation, but cannot represent the same levels of complexities as deep neural networks. Two types of model training have been considered, so called 'frozen' training [155,156] and 'CFD-driven' training [157]. In 'frozen' training closures are developed by using data base information as model inputs and comparing the model predictions, e.g. turbulence stress, to the reference data. This approach is computationally efficient, as evaluating the cost function (which compares the model prediction to reference data) is just an algebraic operation. However, the frozen approach not only requires an adequate amount of data that, if originating from simulations, should be free from numerical errors to perform a meaningful training. This approach also does not guarantee model consistent closures, impairing *a posteriori* model performance.

In the CFD-driven approach, instead, CFD calculations are performed using each candidate closure such that model inputs are obtained from the RANS solution and the data-driven approach receives CFD-feedback. A significant advantage with respect to the frozen approach is the flexibility in the definition of the cost function which now can include any variable of interest. Moreover, it requires much less training data, such as sparse experimentally obtained profiles, not converging candidate models are excluded during training, and the final model, already tested during training, is guaranteed to perform well in *a posteriori* predictions.

As an example, in [158], used a multi-objective version of CFD-driven GEP to ensure that developed models would improve predictions of all key boundary layer metrics in APG and FPG statistically 2D boundary layers, such as the wall-scaled profiles, boundary layer, displacement and momentum thicknesses. Models

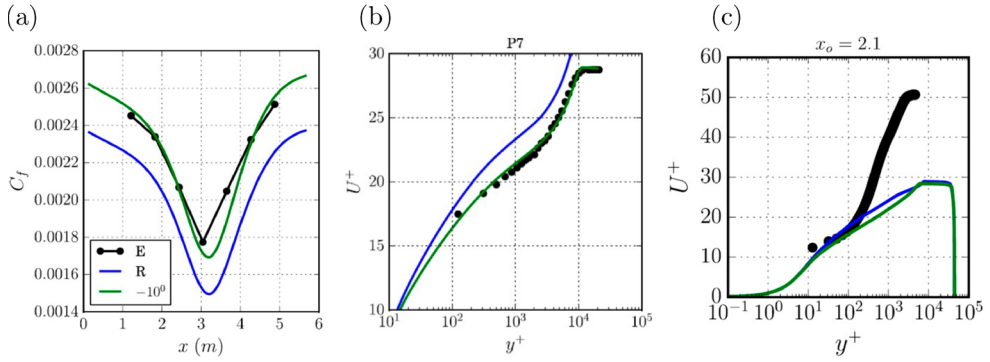

Figure 9. CFD-driven GEP model developed on $\alpha = -10^\circ$ and Re $= 2.5 \times 10^6$ case of VT tunnel data [101], denoted as (-10°), compared with experimental data (E) and baseline RANS (R); C_f (a) and U^+ (b) for $\alpha = 12^\circ$ and Re $= 3.6 \times 10^6$ case of VT tunnel campaign [101]; (c) U^+ at downstream position of experiments with greater PG [159].

resulting from training based on minimising the RANS-prediction error of wall-shear stress *and* boundary-layer displacement were found to consistently improve the prediction over linear turbulence stress closures for all PG cases that had been studied in the VT wind tunnel campaign [101], see examples shown in Figure 9(a,b). Nevertheless, for test cases that feature significantly greater pressure gradient magnitudes [159], i.e. moving further away from conditions the new models were trained on, the new models did not produce better results than linear models, as seen in Figure 9(c), highlighting the importance of having access to training data for very different conditions.

Despite the promising results obtained using 'CFD-driven' modelling, one key downside of this approach is the high computational cost of performing a large number of CFD-evaluations during training. For complex, three-dimensional flow, this makes this approach currently infeasible. Hence, in order to develop new closures for the BeVERLI hill test case [160], we had to revert back to the 'frozen-training' approach. As full volumetric training data was not available for this case, models were instead trained using data from a wall-mounted square cylinder flow, exploiting a new adaptive coefficient capability of the GEP framework to find more accurate constants in the coefficients ξ_n [161]. These models were then tested on the BeVERLI hill test case and showed some improved results over the baseline solution [162], in particular an excellent agreement with experimental data along the centerspan plane ($x = 0$). The centreline plane ($z = 0$) distribution, however, showed an underprediction of C_p on the hill itself and, as a consequence, a recovery downstream of the hill that overshoots the experimental values. Thus, numerical predictions indicate a fully/partially attached flow, while the experiment shows a separated flow, which could be traced back to the trained models providing excessive turbulence kinetic energy production on the hill, as reported in [160].

In summary, data-driven approaches remain a promising tool that are able to improve model predictions in various case studies. Nevertheless, many challenges remain, in particular on how to ensure better generalisability of the models. We observe that model training without CFD-feedback ('frozen' training) does not guarantee better mean flow predictions in *a-posteriori* testing. Further, a critical aspect of this training approach is the availability of volumetric data, which represents a major challenge for high Reynolds number complex geometry flow configurations. On the other hand, while CFD-driven training appears to produce models that perform well in actual CFD, the high computational cost precludes its use for more challenging three-dimensional configurations and thus further work is required to try to reduce the training cost for this approach to become viable.

Wall-Modelled LES (WMLES) improvements are also being investigated. The experiments carried out at Virginia Tech and the USNA, which consider flows in favourable and adverse pressure gradients over smooth and rough walls, are an ideal testing ground for wall models, since the boundary conditions are very well documented. Most models for the wall layer rely on a local equilibrium assumption, justified by the fact that most of the boundary layer is resolved, so that non-equilibrium effects in the outer layer are captured, and that the time-scale of the inner-layer eddies is much smaller than that of the outer-layer ones [57]. The experimental data will be used to evaluate how much non-equilibrium invalidate this assumption, and if more sophisticated models are needed. The experimental measurements of the flow over heterogeneous roughness carried out

at the University of Melbourne are also being considered. Longitudinal vortices are observed at the junction between rough and smooth longitudinal strips [72]. Since these vortices are caused by an imbalance between production and dissipation [79], and such imbalance occurs in the (bypassed) wall-layer, the prediction of these secondary motions is particularly challenging for WMLES.

5. Summary and conclusions

The modelling and prediction of incompressible, non-equilibrium boundary layers at high Reynolds numbers remains a challenging and prevalent problem in naval applications. Our understanding of several of the mechanisms that are concurrently at play is not complete, and accurate models are lacking. This paper has presented some of the salient challenges, discussing our understanding of the respective flow physics and aiming to provide perspective and outlook on ongoing efforts to tackle these challenges.

Surface roughness remains one of these challenges. In equilibrium conditions, outer-layer similarity with smooth wall flows generally holds, when measured carefully and so long as the roughness is sufficiently small compared to the boundary layer thickness. The effect of the roughness can then be reduced to a modified boundary condition for the outer flow, characterised by the roughness function or the equivalent-sand-grain roughness, such that the outer flow can still be resolved using standard methods. The outstanding problem is predicting quantitatively this roughness function, or equivalent sand-grain roughness, from knowledge of the surface topology alone, without actually measuring it in a flow. Most existing predictions rely on the knowledge of the roughness function for sufficiently similar topologies, which can lead to large uncertainties in less explored regions of the parameter space. Physics-based methods that are intrinsically a priori would have the potential to be truly predictive, and we have discussed how there is scope for their development.

In the presence of pressure gradients, there is some evidence that suggests that outer-layer similarity holds for flows with matching histories of β, and therefore the concepts of roughness function and equivalent sand-grain roughness are still useful in these flow configurations. Although the evidence is incomplete, this appears to be the case for FPG flows and at least for moderate APG flows.

Surface topology can be heterogeneous, for instance when roughness presents itself in patches, a situation typical in bio-fouled surfaces and in atmospheric boundary layers. In these cases, equilibrium is disrupted from the wall up and the near-wall flow can prove difficult to model. When roughness changes in the streamwise direction, such as in rough-to-smooth and smooth-to-rough, an analytical, blending model, combining information from the propagation of the new surface conditions in an internal boundary layer and the evolution of the upstream conditions in the original boundary layer, can capture reasonably well the changes in the mean velocity profile and local friction coefficient. In simulations that use wall-models, assuming instantaneous recovery of equilibrium conditions leads to significant errors when estimating the eddy viscosity. The recent LaRTE model, for instance, which accounts for a finite relaxation towards equilibrium after imposing a sudden perturbation in the wall stress, can perform significantly better.

The effect of spanwise heterogeneity is generally more subtle. The imbalance in viscous dissipation over the different regions typically generates large-scale secondary motions in the form of streamwise-aligned rollers. While simulations can qualitatively reproduce such structures, the weak, one-way, coupling between the resolved outer layer and the modelled near-wall region results in weaker rollers, and the velocity deficit over smoother regions is underpredicted. Improved wall models, with stronger coupling between inner and outer layer and a more physical description of the wall eddies, are the focus of ongoing work. Models where the wall layer is populated by synthetic eddies generated using resolvent analysis may be able to improve the inner-outer coupling and result in more accurate predictions.

When focussing on non-equilibrium effects caused by pressure gradients alone, in FPG and weak/mild APG TBLs, the resilience of a logarithmic-like region in the mean velocity was found. RANS modelling for flows with PG should account for this by ensuring that the log-law is not altered in the log-law region. Shielding of the log-law calibration of RANS might be needed, if machine-learning methods are used for a global modification of a RANS model.

At high Reynolds numbers, a lack of data was found for turbulent boundary layers in a significantly strong FPG (remote from the onset of relaminarisation) and in a strong APG (remote from the onset of separation), both in the absence of surface curvature.

New initiatives to generate a data base of non-equilibrium turbulent boundary layer flows involving a systematic variation of the parameters controlling the departure from equilibrium (e.g. families of streamwise pressure gradient distributions) are recommended. Experiments in wind-tunnels and other facilities like towing tanks are needed to achieve high Reynolds numbers. DNS can complement experimental data for small and moderate Reynolds numbers and provide accurate data for the budget of the Reynolds stress equations including the pressure-strain tensor. However, DNS data for high, ship-scale Reynolds numbers cannot be expected during the next few decades.

We have also discussed some of the physical mechanisms at play, the existence or loss of outer-layer similarity, its connection with eddy relaxation times and history effects. We have discussed different modelling efforts, from the focussed detail of the prediction of the roughness function and the equivalent sand-grain roughness to the global picture of the whole flow and its characterisation through different-varying fidelity methods such as RANS or LES, without needing to resolve all the scales in the flow. We have presented progress in the areas of roughness-function prediction, wall functions, closure models using a gene-expression framework, and wall models for LES based on resolvent analysis and in the context of non-equilibrium. The ultimate aim of this work is to pave the way for new paradigms and a new generation of models, which permit accurate yet cost-effective predictions of naval vehicle performances.

Acknowledgments

T. Knopp gratefully acknowledges funding by the DLR internal aeronautical program within the project ADaMant and discussions with P. R. Spalart and A. J. Smits.

Disclosure statement

No potential conflict of interest was reported by the author(s).

Funding

R. García-Mayoral acknowledges the support of EPSRC-UK under grant EP/S013083/1 and AFOSR (EOARD) under grant FA8655-22-1-7062. D. Chung and N. Hutchins acknowledge support from the ARC and from the AFOSR (AOARD) under grant FA2386-21-1-4018. R. Sandberg acknowledges support from the ARC and from the U.S. Office of Naval Research (ONR) under NICOP Grant N62909-20-1-2046 with program monitors program monitors Elena McCarthy (ONR-G), Yin Lu (Julie) Young (ONR). U. Piomelli acknowledges the support of the Natural Sciences and Engineering Research Council, under the Discovery Grant program. P. Durbin acknowledges support from the Office of Naval Research under grant N00014-17-1-2200 with program monitor Peter Chang. B. McKeon acknowledges support from the Office of Naval Research under grants N00014-17-1-2307 and N00014-17-1-2960 (program monitor Peter Chang) and N00014-17-1-3022 (program monitor Ellen Livingstone).

References

[1] Toxopeus SL, Bettle MC, Uroić T. NATO AVT-301 collaborative exercise: CFD predictions for BB2 generic submarine, phase 0–pre-test computations. In: NATO STO AVT-307 Research Symposium on Separated Flow: Prediction, Measurement and Assessment for Air and Sea Vehicles; Oct.; Trondheim, Norway; 2019. STO-TR-AVT-307-22.
[2] Clauser F. The turbulent boundary layer. Adv Appl Mech. 1956;4:1–51. doi: 10.1016/S0065-2156(08)70370-3
[3] Hama FR. Boundary layer characteristics for smooth and rough surfaces. Trans Soc Nav Arch Marine Engrs. 1954;62:333–358.
[4] Andersson J, Oliveira DR, Yeginbayeva I, et al. Review and comparison of methods to model ship hull roughness. Appl Ocean Res. 2020;99:102119. doi: 10.1016/j.apor.2020.102119
[5] Chung D, Hutchins N, Schultz MP, et al. Predicting the drag of rough surfaces. Annu Rev Fluid Mech. 2021;53(1):439–471. doi: 10.1146/fluid.2020.53.issue-1
[6] Moody LF. Friction factors for pipe flow. Trans ASME. 1944;66(8):671–684.
[7] Bradshaw P. A note on "critical roughness height" and "transitional roughness". Phys Fluids. 2000;12(6):1611–1614. doi: 10.1063/1.870410
[8] Nikuradse J. Strömungsgesetze in rauhen rohren. VDI-Forschungsheft. 1933;361:1.
[9] Monty JP, Dogan E, Hanson R, et al. An assessment of the ship drag penalty arising from light calcareous tubeworm fouling. Biofouling. 2016;32(4):451–464. doi: 10.1080/08927014.2016.1148140
[10] Flack K, Schultz M, Barros J, et al. Skin-friction behavior in the transitionally-rough regime. Int J Heat Fluid Flow. 2016;61:21–30. doi: 10.1016/j.ijheatfluidflow.2016.05.008

[11] Thakkar M, Busse A, Sandham ND. Direct numerical simulation of turbulent channel flow over a surrogate for Nikuradse-type roughness. J Fluid Mech. 2018;837:R1. doi: 10.1017/jfm.2017.873
[12] Chan L, MacDonald M, Chung D, et al. A systematic investigation of roughness height and wavelength in turbulent pipe flow in the transitionally rough regime. J Fluid Mech. 2015;771:743–777. doi: 10.1017/jfm.2015.172
[13] Abderrahaman-Elena N, Fairhall CT, García-Mayoral R. Modulation of near-wall turbulence in the transitionally rough regime. J Fluid Mech. 2019;865:1042–1071. doi: 10.1017/jfm.2019.41
[14] Volino R, Fritch D, Devenport W, et al. Effects of roughness on non-equilibrium turbulent boundary layers. J Turb. 2024. doi: 10.1080/14685248.2024.2360186
[15] Fairhall CT, Abderrahaman-Elena N, García-Mayoral R. The effect of slip and surface texture on turbulence over superhydrophobic surfaces. J Fluid Mech. 2019;861:88–118. doi: 10.1017/jfm.2018.909
[16] Bottaro A. Flow over natural or engineered surfaces: an adjoint homogenization perspective. J Fluid Mech. 2019;877:P1. doi: 10.1017/jfm.2019.607
[17] Hao Z, García-Mayoral R. Turbulent flows over porous/rough walls: response of velocity to stress on surfaces. In: 75th Annual Meeting of the Division of Fluid Dynamics; Indianapolis, US. 2022.
[18] Hao Z, García-Mayoral R. Turbulent flows over porous and rough substrates. arXiv:240215244. 2024. p. 1–37.
[19] Xie W, Fairhall CT, García-Mayoral R. Resolving turbulence and drag over textured surfaces using texture-less simulations: the case of slip/no-slip textures. arXiv:240405926. 2024. p. 1–33.
[20] Varghese J, Durbin PA. Representing surface roughness in eddy resolving simulation. J Fluid Mech. 2020;897:A10. doi: 10.1017/jfm.2020.368
[21] Durbin PA, Medic G, Seo JM, et al. Rough wall modification of two-layer k-ϵ. J Fluids Eng. 2001;123(1):16–21. doi: 10.1115/1.1343086
[22] Aupoix B, Spalart P. Extensions of the Spalart–Allmaras turbulence model to account for wall roughness. Int J Heat Fluid Flow. 2003 Aug;24(4):454–462. doi: 10.1016/s0142-727x(03)00043-2
[23] Knopp T, Eisfeld B, Calvo JB. A new extension for k-ω turbulence models to account for wall roughness. Int J Heat Fluid Flow. 2009;30(1):54–65. doi: 10.1016/j.ijheatfluidflow.2008.09.009
[24] Aupoix B. Roughness corrections for the k-ω shear stress transport model: status and proposals. J Fluids Eng. 2015;137(2):021202. doi: 10.1115/1.4028122
[25] Eça L, Kerkvliet M, Starke AR, et al. A verification and validation study of RANS based roughness models at model and full scale Reynolds numbers. In: 35th Symposium on Naval Hydrodynamics. Nantes, France; 2024.
[26] Pullin DI, Hutchins N, Chung D. Turbulent flow over a long flat plate with uniform roughness. Phys Rev Fluids. 2017;2(8):082601. doi: 10.1103/PhysRevFluids.2.082601
[27] Utama IKAP, Nugroho B, Yusuf M, et al. The effect of cleaning and repainting on the ship drag penalty. Biofouling. 2021 Apr;37(4):372–386. doi: 10.1080/08927014.2021.1914599
[28] Hutchins N, Ganapathisubramani B, Schultz M, et al. Defining an equivalent homogeneous roughness length for turbulent boundary layers developing over patchy or heterogeneous surfaces. Ocean Eng. 2023;271:113454. doi: 10.1016/j.oceaneng.2022.113454
[29] Breugem WP, Boersma BJ, Uittenbogaard RE. The influence of wall permeability on turbulent channel flow. J Fluid Mech. 2006;562:35–72. doi: 10.1017/S0022112006000887
[30] Suga K, Matsumura Y, Ashitaka Y, et al. Effects of wall permeability on turbulence. Int J Heat Fluid Flow. 2010;31(6):974–984. doi: 10.1016/j.ijheatfluidflow.2010.02.023
[31] Manes C, Poggi D, Ridolfi L. Turbulent boundary layers over permeable walls: scaling and near-wall structure. J Fluid Mech. 2011;687:141–170. doi: 10.1017/jfm.2011.329
[32] Kuwata Y, Suga K. Direct numerical simulation of turbulence over anisotropic porous media. J Fluid Mech. 2017;831:41–71. doi: 10.1017/jfm.2017.619
[33] Fang H, Han X, He G, et al. Influence of permeable beds on hydraulically macro-rough flow. J Fluid Mech. 2018;847:552–590. doi: 10.1017/jfm.2018.314
[34] Shen G, Yuan J, Phanikumar MS. Direct numerical simulations of turbulence and hyporheic mixing near sediment–water interfaces. J Fluid Mech. 2020;892:A20. doi: 10.1017/jfm.2020.173
[35] Kazemifar F, Blois G, Aybar M, et al. The effect of biofilms on turbulent flow over permeable beds. Water Resour Res. 2021;57(2):e2019WR026032. doi: 10.1029/2019WR026032
[36] Okazaki Y, Takase Y, Kuwata Y, et al. Describing characteristic parameters of turbulence over two-dimensional porous roughness. J Therm Sci Technol. 2021;16(2):JTST0027–JTST0027. doi: 10.1299/jtst.2021jtst0027
[37] Okazaki Y, Takase Y, Kuwata Y, et al. Turbulent channel flows over porous rib-roughed walls. Exp Fluids. 2022;63(4):1–20. doi: 10.1007/s00348-022-03415-8
[38] Endrikat S, Newton R, Modesti D, et al. Reorganisation of turbulence by large and spanwise-varying riblets. J Fluid Mech. 2022 Nov;952:A27. doi: 10.1017/jfm.2022.897
[39] Karra SK, Apte SV, He X, et al. Pore-resolved investigation of turbulent open channel flow over a randomly packed permeable sediment bed. J Fluid Mech. 2023;971:A23. doi: 10.1017/jfm.2023.636
[40] Mizuno Y, Jiménez J. Wall turbulence without walls. J Fluid Mech. 2013 Apr;723:429–455. doi: 10.1017/jfm.2013.137
[41] Kwon Y, Jiménez J. An isolated logarithmic layer. J Fluid Mech. 2021 Apr;916:A35. doi: 10.1017/jfm.2021.177

[42] Jiménez J. Turbulent flows over rough walls. Ann Rev Fluid Mech. 2004;36:173–196. doi: 10.1146/fluid.2004.36.issue-1
[43] Volino RJ, Schultz MP. Effects of boundary layer thickness on the estimation of equivalent sandgrain roughness in zero-pressure-gradient boundary layers. Exp Fluids. 2022;63(8):131. doi: 10.1007/s00348-022-03479-6
[44] Durbin PA. Reflections on roughness modelling in turbulent flow. J Turbul. 2022;24(1-2):3–13. doi: 10.1080/14685248.2022.2137171
[45] Flack KA, Schultz MP, Connelly JS. Examination of a critical roughness height for outer layer similarity. Phys Fluids. 2007;19(9):095104. doi: 10.1063/1.2757708
[46] Li Q, Bou-Zeid E, Anderson W, et al. Quality and reliability of LES of convective scalar transfer at high reynolds numbers. Int J Heat Mass Transf. 2016 Nov;102:959–970. doi: 10.1016/j.ijheatmasstransfer.2016.06.093
[47] Li Q, Bou-Zeid E. Contrasts between momentum and scalar transport over very rough surfaces. J Fluid Mech. 2019 Oct;880:32–58. doi: 10.1017/jfm.2019.687
[48] MacDonald M, Ooi A, Garcıa-Mayoral R, et al. Direct numerical simulation of high aspect ratio spanwise-aligned bars. J Fluid Mech. 2018 Mar;843:126–155. doi: 10.1017/jfm.2018.150
[49] Sharma A, García-Mayoral R. Turbulent flows over dense filament canopies. J Fluid Mech. 2020;888:A2.
[50] Chen Z, García-Mayoral R. Examination of outer-layer similarity in wall turbulence over obstructing surfaces. J Fluid Mech. 2023;973:A31. doi: 10.1017/jfm.2023.792
[51] Garcıa-Mayoral R, Jiménez J. Scaling of turbulent structures in riblet channels up to $\mathrm{Re}_\tau \approx 550$. Physics of Fluids. 2012;24(10):105101.
[52] Yuan J, Piomelli U. Numerical simulations of sink-flow boundary layers over rough surfaces. Phys Fluids. 2014;26:0151130151–28015113–1–28 .
[53] Yuan J, Piomelli U. Numerical simulation of a spatially developing accelerating boundary layer over roughness. J Fluid Mech. 2015;780:192–214. doi: 10.1017/jfm.2015.437
[54] Wu W, Piomelli U. Effects of surface roughness on a separating turbulent boundary layer. J Fluid Mech. 2018;841:552–580. doi: 10.1017/jfm.2018.101
[55] Bou-Zeid E, Anderson W, Katul GG, et al. The persistent challenge of surface heterogeneity in boundary-layer meteorology: A review. Boundary Layer Meteorol. 2020;177(2-3):227–245. doi: 10.1007/s10546-020-00551-8
[56] Li M, de Silva CM, Rouhi A, et al. Recovery of wall-shear stress to equilibrium flow conditions after a rough-to-smooth step change in turbulent boundary layers. J Fluid Mech. 2019;872:472–491. doi: 10.1017/jfm.2019.351
[57] Larsson J, Kawai S, Bodart J, et al. Large eddy simulation with modeled wall-stress: recent progress and future directions. Mech Eng Rev. 2016;3(1):1–23. doi: 10.1299/mer.15-00418
[58] Li M, de Silva CM, Chung D, et al. Modelling the downstream development of a turbulent boundary layer following a step change of roughness. J Fluid Mech. 2022;949:A7. doi: 10.1017/jfm.2022.731
[59] Antonia RA, Luxton RE. The response of a turbulent boundary layer to a step change in surface roughness. Part 1. Smooth to rough. J Fluid Mech. 1971;48(4):721–761. doi: 10.1017/S0022112071001824
[60] Antonia RA, Luxton RE. The response of a turbulent boundary layer to a step change in surface roughness. Part 2. Rough to smooth. J Fluid Mech. 1972;53(4):737–757. doi: 10.1017/S002211207200045X
[61] Ismail U, Zaki TA, Durbin PA. Simulations of rib-roughened rough-to-smooth turbulent channel flows. J Fluid Mech. 2018;843:419–449. doi: 10.1017/jfm.2018.119
[62] Ismail U, Zaki TA, Durbin PA. The effect of cube-roughened walls on the response of rough-to-smooth (rts) turbulent channel flows. Int J Heat Fluid Flow. 2018;72:174–185. doi: 10.1016/j.ijheatfluidflow.2018.05.008
[63] Rouhi A, Chung D, Hutchins N. Direct numerical simulation of open-channel flow over smooth-to-rough and rough-to-smooth step changes. J Fluid Mech. 2019;866:450–486. doi: 10.1017/jfm.2019.84
[64] Li M, de Silva CM, Chung D, et al. Experimental study of a turbulent boundary layer with a rough-to-smooth change in surface conditions at high reynolds numbers. J Fluid Mech. 2021;923:A18. doi: 10.1017/jfm.2021.577
[65] Chamorro LP, Porté-Agel F. Velocity and surface shear stress distributions behind a rough-to-smooth surface transition: a simple new model. Boundary Layer Meteorol. 2009;130(1):29–41. doi: 10.1007/s10546-008-9330-x
[66] Rouhi A, Chung D, Hutchins N. Roughness and reynolds number effects on the flow past a rough-to-smooth step change. In: iTi Conference on Turbulence. Springer; 2018. p. 81–86.
[67] van Driest ER. On turbulent flow near a wall. J Aero Sci. 1956;23:1007–1011. doi: 10.2514/8.3713
[68] Thorsness C, Morrisroe P, Hanratty T. A comparison of linear theory with measurements of the variation of shear stress along a solid wave. Chem Eng Sci. 1978;33(5):579–592. doi: 10.1016/0009-2509(78)80020-7
[69] Luchini P, Charru F. On the large difference between benjamin's and hanratty's formulations of perturbed flow over uneven terrain. J Fluid Mech. 2019;871:534–561. doi: 10.1017/jfm.2019.312
[70] Chedevergne F, Stuck M, Olazabal-Loumé M, et al. About the role of the hanratty correction in the linear response of a turbulent flow bounded by a wavy wall. J Fluid Mech. 2023;967:A39. doi: 10.1017/jfm.2023.507
[71] Salomone T, Piomelli U, De Stefano G. Wall-modeled and hybrid large-eddy simulations of the flow over roughness strips. Fluids. 2022 Dec;8(1):10. doi: 10.3390/fluids8010010
[72] Wangsawijaya DD, Baidya R, Chung D, et al. The effect of spanwise wavelength of surface heterogeneity on turbulent secondary flows. J Fluid Mech. 2020;894:A7A1–36A7–1–36 . doi: 10.1017/jfm.2020.262
[73] Meneveau C. A note on fitting a generalised Moody diagram for wall modelled large-eddy simulations. J Turbul. 2020;21(11):650–673. doi: 10.1080/14685248.2020.1840573

[74] Travin AK, Shur ML, Spalart PR, et al. Improvement of delayed detached-eddy simulation for LES with wall modelling. In: Wesseling P, Oñate E, Pèriaux J, editors. European Conference on Computational Fluid Dynamics ECCOMAS CFD 2006. TU Delft; 2006. p. 410–432.
[75] Fowler M, Zaki TA, Meneveau C. A Lagrangian relaxation towards equilibrium wall model for large eddy simulation. J Fluid Mech. 2022;934:A44. doi: 10.1017/jfm.2021.1156
[76] Fowler M, Zaki TA, Meneveau C. A multi-timescale wall model for LES and applications to non-equilibrium channel flows. J Fluid Mech. 2023;974:A51. doi: 10.1017/jfm.2023.585
[77] Stroh A, Schäfer K, Frohnapfel B, et al. Rearrangement of secondary flow over spanwise heterogeneous roughness. J Fluid Mech. 2020;885:R5. doi: 10.1017/jfm.2019.1030
[78] Schäfer K, Stroh A, Forooghi P, et al. Modelling spanwise heterogeneous roughness through a parametric forcing approach. J Fluid Mech. 2022;930:A7. doi: 10.1017/jfm.2021.850
[79] Hinze JO. Secondary currents in wall turbulence. Phys Fluids. 1967;10:S122–S125. doi: 10.1063/1.1762429
[80] McKeon BJ, Sharma AS. A critical-layer framework for turbulent pipe flow. J Fluid Mech. 2010;658:336–382. doi: 10.1017/S002211201000176X
[81] Sharma AS, Moarref R, McKeon BJ, et al. Low-dimensional representations of exact coherent states of the Navier-Stokes equations from the resolvent model of wall turbulence. Phys Rev E. 2016;93(2):021102. doi: 10.1103/PhysRevE.93.021102
[82] Spalart PR. Philosophies and fallacies in turbulence modeling. Prog Aerosp Sci. 2015;74:1–15. doi: 10.1016/j.paerosci.2014.12.004
[83] Devenport WJ, Lowe KT. Equilibrium and non-equilibrium turbulent boundary layers. Prog Aerosp Sci. 2022;131:100807. doi: 10.1016/j.paerosci.2022.100807
[84] Clauser FH. Turbulent boundary layers in adverse pressure gradients. J Aeronaut Sci. 1954;21:91–108. doi: 10.2514/8.2938
[85] Elsberry K, Loeffler J, Zhou MD, et al. An experimental study of a boundary layer that is maintained on the verge of separation. J Fluid Mech. 2000;423:227–261. doi: 10.1017/S0022112000001828
[86] Hinze JO. Experimental investigation on secondary currents in the turbulent flow through a straight conduit. Appl Sci Res. 1973;28(1):453–465. doi: 10.1007/BF00413083
[87] Kader BA, Yaglom AM. Similarity treatment of moving-equilibrium turbulent boundary layers in adverse pressure gradients. J Fluid Mech. 1978;89:305–342. doi: 10.1017/S0022112078002621
[88] Durbin PA, Reif BAP. Statistical theory and modelling for turbulent flows. Chichester: John Wiley & Sons; 2001.
[89] Eisfeld B. The importance of turbulent equilibrium for Reynolds-stress modeling. Phys Fluids. 2022;34:0251230251-12025123-1–12. doi: 10.1063/5.0081157
[90] Eisfeld B. Characteristics of incompressible free shear flows and implications for turbulence modeling. AIAA J. 2021;59:180–195. doi: 10.2514/1.J059654
[91] Wilcox DC. Turbulence modeling for CFD. La Canada: DWC Industries; 1998.
[92] Knopp T, Reuther N, Novara M, et al. Experimental analysis of the log law at adverse pressure gradient. J Fluid Mech. 2021;918:A17. doi: 10.1017/jfm.2021.331
[93] Rotta J. Über die Theorie turbulenter Grenzschichten. Mitteilungen aus dem Max-Planck-Institut für Strömungsforschung Nr. 1. (Translated as: On the theory of turbulent boundary layers. NACA Technical Memorandum No. 1344, 1953.); 1950.
[94] Klewicki J, Sandberg R, Knopp T, et al. On the physical structure, modeling and computation-Based prediction of two-Dimensional, smooth-Wall turbulent boundary layers subjected to streamwise pressure gradients. J Turb. 2024;X. cross–reference in this volume
[95] Coles DE, Hirst EA. Computation of Turbulent Boundary Layers – 1968 AFOSR-IFP-Stanford Conference. Thermosciences Division, Department of Mechanical Engineering, Stanford University; 1969.
[96] Alving AE, Fernholz HH. Mean-velocity scaling in and around a mild, turbulent separation bubble. Phys Fluids. 1995;7:1956–1969. doi: 10.1063/1.868772
[97] Johnstone R, Coleman GN, Spalart PR. The resilience of the logarithmic law to pressure gradients: evidence from direct numerical simulation. J Fluid Mech. 2010;643:163–175. doi: 10.1017/S0022112009992333
[98] Webster D, DeGraaff D, Eaton J. Turbulence characteristics of a boundary layer over a two-dimensional bump. J Fluid Mech. 1996;320:53–69. doi: 10.1017/S0022112096007458
[99] Bourassa C, Thomas FO. An experimental investigation of a highly accelerated turbulent boundary layer. J Fluid Mech. 2009;634:359–404. doi: 10.1017/S0022112009007289
[100] Spalart PR. The law of the wall. Indications from DNS, and opinion. In: Stanislas M, Jimenez J, Marusic I, editors. Progress in wall turbulence: understanding and modelling. Proceedings of the WALLTURB International Workshop held in Lille, France, April 21–23, 2009. Springer; 2010. p. 9–20; ERCOFTAC Series.
[101] Fritsch D, Vishwanathan V, Roy CJ, et al. Experimental and computational study of 2D smooth wall turbulent boundary layers in pressure gradient. In: AIAA SCITECH 2022 Forum; San Diego, US. 2022. p. 0696.
[102] Knopp T. An empirical wall law for the mean velocity in an adverse pressure gradient for RANS turbulence modelling. Flow Turbul Combust. 2022;109:571–601. doi: 10.1007/s10494-022-00367-1
[103] Nickels TB. Inner scaling for wall-bounded flows subject to large pressure gradients. J Fluid Mech. 2004;521:217–239. doi: 10.1017/S0022112004001788

[104] Dixit SA, Ramesh ON. Pressure-gradient-dependent logarithmic laws in sink flow turbulent boundary layers. J Fluid Mech. 2008;615:445–475. doi: 10.1017/S0022112008004047
[105] Knopp T. A new wall-law for adverse pressure gradient flows and modification of k-ω type RANS turbulence models. In: 54th AIAA Aerospace Sciences Meeting. American Institute of Aeronautics and Astronautics; San Diego, US. 2016.
[106] Sporschill G. Improved Reynolds-stress modeling for adverse-pressure-gradient turbulent boundary layers in industrial aeronautical flow [dissertation]. École doctorale sciences exactes et leurs applications (Pau, Pyrénées Atlantiques). and Laboratoire de mathématiques et de leurs applications (Pau). and Dassault Aviation; 2021.
[107] Telbany MMME, Reynolds AJ. Velocity distributions in plane turbulent channel flows. J Fluid Mech. 1980;100(01):1. doi: 10.1017/S0022112080000973
[108] Nakabayashi K, Kitoh O, Katoh Y. Similarity laws of velocity profiles and turbulence characteristics of Couette-Poiseuille turbulent flows. J Fluid Mech. 2004;507:43-–69. doi: 10.1017/S0022112004008110
[109] Gungor AG, Maciel Y, Simens MP, et al. Scaling and statistics of large-defect adverse pressure gradient turbulent boundary layer. Int J Heat Fluid Flow. 2016;59:109–124. doi: 10.1016/j.ijheatfluidflow.2016.03.004
[110] Perry AE, Marusic I, Jones MB. On the streamwise evolution of turbulent boundary layers in arbitrary pressure gradients. J Fluid Mech. 2002;461:61–91. doi: 10.1017/S002211200200825X
[111] Perry AE. Turbulent boundary layers in decreasing adverse presssure gradients. J Fluid Mech. 1966;25:481–506. doi: 10.1017/S0022112066001344
[112] Perry AE, Bell JB, Joubert PN. Velocity and temperature profiles in adverse pressure gradient turbulent boundary layers. J Fluid Mech. 1966;25:299–320. doi: 10.1017/S0022112066001666
[113] Romero SK, Zimmerman SJ, Philip J, et al. Properties of the inertial sublayer in adverse pressure-gradient turbulent boundary layers. J Fluid Mech. 2022;937:A30A31–36A30–1–36 . doi: 10.1017/jfm.2022.6
[114] Stratford BS. The prediction of separation of the turbulent boundary layer. J Fluid Mech. 1959;5:1–16. doi: 10.1017/S0022112059000015
[115] Rao MS, Hassan HA. Modeling turbulence in the presence of adverse pressure gradients. J Aircraft. 1998;35(3):500–502.
[116] Catris S, Aupoix B. Towards a calibration of the length-scale equation. Int J Heat Fluid Flow. 2000;21(5):606–613.
[117] Knopp T. Modification of the SSG/LRR-Omega model for turbulent boundary layers in an adverse pressure gradients. Flow Turbul Combust. 2022;111:409–438. doi: 10.1007/s10494-023-00457-8
[118] Skare PE, Krogstad PA. A turbulent equilibrium boundary layer near separation. J Fluid Mech. 1994;272:319–348. doi: 10.1017/S0022112094004489
[119] Smits AJ, Wood DH. The response of turbulent boundary layers to sudden perturbations. Ann Rev Fluid Mech. 1985;17:321–358. doi: 10.1146/fluid.1985.17.issue-1
[120] Bradshaw P. Effects of streamline curvature on turbulent flow. AGARDograph 169; 1973.
[121] Smits AJ, Young STB, Bradshaw P. The effect of short regions of high surface curvature on turbulent boundary layers. J Fluid Mech. 1979;94:209–242. doi: 10.1017/S0022112079001002
[122] Sillero JA, Jiménez J, Moser RD. One-point statistics for turbulent wall-bounded flows at Reynolds numbers up to $\delta^+ \approx 2000$. Phys Fluids. 2013;25:105102. doi: 10.1063/1.4823831
[123] Marusic I, Chauhan KA, Kulandaivelu V, et al. Evolution of zero-pressure-gradient boundary layers from different tripping conditions. J Fluid Mech. 2015;783:379–411. doi: 10.1017/jfm.2015.556
[124] Olsen ME, Coakley TJ, Lillard RP. The lag model applied to high speed flows. AIAA Paper 2005; 2005-101.
[125] Biswas R, Durbin PA. Assessment of viscosity models that incorporate lag parameter scaling. Int J Heat Fluid Flow. 2019;78:1084271081–19108427–1–19 . doi: 10.1016/j.ijheatfluidflow.2019.108427
[126] Hamlington PE, Ihme M. Modeling of non-equilibrium homogeneous turbulence in rapid compressed flows. Flow Turbul Combust. 2014;93:93-–124. doi: 10.1007/s10494-014-9535-7
[127] Eça L, Kerkvliet M, Toxopeus SL. Comparison of RANS turbulence models for the simulation of smooth wall boundary-layers in pressure gradients at moderate and high Reynolds numbers. In: X International Conference on Computational Methods in Marine Engineering (MARINE); Madrid, Spain. 2023.
[128] Knopp T, Eça L, Toxopeus SL, et al. Errors and uncertainties in CFD validation for non-equilibrium turbulent boundary layer flows at high Reynolds numbers. J Turb. 2024;X. cross–reference in this volume.
[129] Cal RB, Castillo L. Similarity analysis of favorable pressure gradient turbulent boundary layers with eventual quasilaminarization. Phys Fluids. 2008;20:1051061051–18105106–1–18 . doi: 10.1063/1.2991433
[130] Ranjan R, Narasimha R. An assessment of the two-layer quasi-laminar theory of relaminarisation through recent high-re accelerated turbulent boundary layer experiments. J Fluids Eng. 2017;139:111205. doi: 10.1115/1.4037059
[131] Joshi P, Liu X, Katz J. Effect of mean and fluctuating pressure gradients on boundary layer turbulence. J Fluid Mech. 2014;748:36–84. doi: 10.1017/jfm.2014.147
[132] Bobke A, Vinuesa R, Örlü R, et al. History effects and near equilibrium in adverse-pressure-gradient turbulent boundary layers. J Fluid Mech. 2017;820:667–692. doi: 10.1017/jfm.2017.236
[133] Vinuesa R, Örlü R, Vila CS, et al. Revisiting history effects in adverse-pressure-gradient turbulent boundary layers. Flow Turbul Combust. 2017;99:565–587. doi: 10.1007/s10494-017-9845-7

[134] Metin C, Gungor TR, Simens MP, et al. How history effects influence favourable pressure gradient turbulent boundary layers. In: APS Division of Fluid Dynamics (Fall) 2020, abstract id.P14.004; Chicago, US. 2020.
[135] Samuel AE, Joubert PN. A boundary layer developing in an increasingly adverse pressure gradient. J Fluid Mech. 1974;66:481–505. doi: 10.1017/S0022112074000322
[136] Ambrogi F, Piomelli U, Rival DE. Characterization of unsteady separation in a turbulent boundary layer. J Fluid Mech. 2022;945(A10):1–30.
[137] Ambrogi F, Piomelli U, Rival DE. Characterization of unsteady separation in a turbulent boundary layer: Reynolds stresses and flow dynamics. J Fluid Mech. 2023;972(A36):1–24.
[138] MacDougall CY, Piomelli U, Ambrogi F. Evaluation of turbulence models in unsteady separation. Fluids. 2023;8(273):1–17.
[139] Eça L, Kerkvliet M, Toxopeus SL. Attaining the asymptotic range in RANS simulations. In: ASME Verification, Validation and Uncertainty Quantification Symposium (VVUQ); Baltimore (MD); 2023. VVUQ2023-108745.
[140] Alving AE, Smits AJ, Watmuff JH. Turbulent boundary layer relaxation from convex curvature. J Fluid Mech. 1990;211:529–556. doi: 10.1017/S0022112090001689
[141] Parthasarathy A, Saxton-Fox T. A family of adverse pressure gradient turbulent boundary layers with upstream favourable pressure gradients. J Fluid Mech. 2023;966:A11A11–29A11–1–29 . doi: 10.1017/jfm.2023.429
[142] Pope SB. Turbulent flows. Cambridge: Cambridge University Press; 2000.
[143] Gleize V, Schiestel R, Couaillier V. Multiple scale modeling of turbulent nonequilibrium boundary layer flows. Phys Fluids. 1996;8:2716–2732. doi: 10.1063/1.869058
[144] Rodi W. A new algebraic relation for calculating the Reynolds stresses. In: Gesellschaft Angewandte Mathematik und Mechanik Workshop Paris France; Vol. 56; Goettingen, Germany. 1976. p. 219.
[145] Pope S. A more general effective-viscosity hypothesis. J Fluid Mech. 1975;72(2):331–340. doi: 10.1017/S0022112075003382
[146] Schmelzer M, Dwight RP, Cinnella P. Discovery of algebraic Reynolds-stress models using sparse symbolic regression. Flow Turbul Combust. 2020;104(2):579–603. doi: 10.1007/s10494-019-00089-x
[147] Gatski TB, Speziale CG. On explicit algebraic stress models for complex turbulent flows. J Fluid Mech. 1993;254:59–78. doi: 10.1017/S0022112093002034
[148] Wallin S, Johansson AV. An explicit algebraic Reynolds stress model for incompressible and compressible turbulent flows. J Fluid Mech. 2000;403:89–132. doi: 10.1017/S0022112099007004
[149] Ling J, Kurzawski A, Templeton J. Reynolds averaged turbulence modelling using deep neural networks with embedded invariance. J Fluid Mech. 2016;807:155–166. doi: 10.1017/jfm.2016.615
[150] Duraisamy K, Iaccarino G, Xiao H. Turbulence modeling in the age of data. Annu Rev Fluid Mech. 2019;51:357–377. doi: 10.1146/fluid.2019.51.issue-1
[151] Sandberg RD, Zhao Y. Machine-learning for turbulence and heat-flux model development: A review of challenges associated with distinct physical phenomena and progress to date. Int J Heat Fluid Flow. 2022;95:108983. doi: 10.1016/j.ijheatfluidflow.2022.108983
[152] Fukami K, Fukagata K, Taira K. Assessment of supervised machine learning methods for fluid flows. Theor Comput Fluid Dyn. 2020;34:497–519. doi: 10.1007/s00162-020-00518-y
[153] Duraisamy K, Spalart PR, Rumsey CL. Status, emerging ideas and future directions of turbulence modeling research in aeronautics. NASA; 2017.
[154] Rumsey C, Coleman G. NASA symposium on turbulence modeling: roadblocks, and the potential for machine learning. NASA; 2022.
[155] Weatheritt J, Sandberg RD. A novel evolutionary algorithm applied to algebraic modifications of the RANS stress–strain relationship. J Comput Phys. 2016;325:22–37. doi: 10.1016/j.jcp.2016.08.015
[156] Weatheritt J, Sandberg RD. Improved junction body flow modeling through data-driven symbolic regression. J Ship Res. 2019;63(4):283–293. doi: 10.5957/JOSR.09180053
[157] Zhao Y, Akolekar HD, Weatheritt J, et al. RANS turbulence model development using CFD-driven machine learning. J Comput Phys. 2020;411:109413. doi: 10.1016/j.jcp.2020.109413
[158] Lav C, Sandberg RD. CFD-driven machine-learning using sparse experimental data of smooth-wall turbulent boundary layers under pressure gradients. In: 34th Symposium on Naval Hydrodynamics. Washington (DC); 2022. p. 1–13.
[159] Bross M, Fuchs T, Kähler CJ. Interaction of coherent flow structures in adverse pressure gradient turbulent boundary layers. J Fluid Mech. 2019;873:287–321. doi: 10.1017/jfm.2019.408
[160] Lowe KT, Smits A, Visonneau M, et al. Effects of streamline curvature and three dimensionality. J Turb. 2024;X. cross–reference in this volume.
[161] Waschkowski F, Li H, Deshmukh A, et al. Gradient information and regularization for gene expression programming to develop data-driven physics closure models. arXiv preprint arXiv:221112341. 2022.
[162] Gargiulo A, Ozoroski TA, Hallock T, et al. Computations of the BeVERLI hill three-dimensional separating flow model validation cases. In: AIAA Science and Technology Forum; San Diego (CA), USA; 3–7 Jan 2022.